1973

Secondary emission of chalcogenide glasses

Steven Richard Doctor
Iowa State University

Secondary emission of chalcogenide glasses

by

Steven Richard Doctor

A Dissertation Submitted to the
Graduate Faculty in Partial Fulfillment of
The Requirements for the Degree of
DOCTOR OF PHILOSOPHY

Major: Electrical Engineering

Approved:

Signature was redacted for privacy.

In Charge of Major Work

Signature was redacted for privacy.

For the Major Department

Signature was redacted for privacy.

For the Graduate College

Iowa State University
Ames, Iowa

1973

TABLE OF CONTENTS

LIST OF TABLES

LIST OF FIGURES

I. INTRODUCTION

A. Historical Information

The development of computers had, by the middle 1950's reached the state where large scale general-purpose electronic digital computers were an actuality. The need for large storage capacity was met by three devices: delay lines, magnetic drums, and electrostatic storage tubes. All three of these devices were used in commercial machines. See Richards (21) for a detailed comparison of the advantages and disadvantages of each.

In electrostatic storage there were four types of tubes that were developed. All of these tubes stored information in a pattern on an insulator. These tubes were referred to as the Williams tube, the Selectron, the holding-gun tube and the barrier-grid tube. These were developed from the already established cathode ray tube technology that had been developed for television and oscilloscope applications. The Williams tube consists of a cathode ray tube, a pickup plate, an amplifier, logic circuits, and deflection and grid control circuits. It stored on the order of 1000 bits per tube. The cycle time was approximately 8 microseconds per bit. With this tube the information had to be regenerated periodically because the insulating material, on the back side of the face of the tube,was imperfect and this caused

the charge pattern to be destroyed. Typically, every third cycle was set aside for regeneration and the computer did not have access to the storage system during this time. The cathode ray tubes had to be modified to obtain a very small beam diameter at all points on the storage surface and for the elimination of blemishes on the storage surface. To minimize the beam diameter the distance between the electron gun and the storage surface was reduced but then deflection defocusing became a troublesome phenomena. Also, the small beam diameter limited the beam current density.

The barrier-grid storage tube differed from the Williams tube only in that the pickup plate was in physical contact with the electrostatic storage surface (hence, it is called a back plate) and there were two screens in front of the storage surface. The one nearest the storage surface is called the barrier grid and it is at ground potential. The other one is referred to as the collector grid and it is at a positive potential of typically 250 volts. This tube could store approximately 10,000 bits. Only after interrogating a single bit 100 times did the adjacent bits need to be regenerated. These two factors were great improvements over the Williams tubes. The disadvantage of increased manufacturing costs made them attractive only in large quantities.

The holding gun tube was developed to eliminate the need for regeneration. This differed from the Williams tube

by having a back plate, a collector grid at ground potential, and a holding gun with its cathode at some negative potential. The storage capacity and the access time properties are about the same as for the Williams tube. This tube and the barrier-grid tube use a group of cells to store a single bit of information. This provides a large output signal upon interrogation and aids the compromise between beam diameter, deflection defocusing and beam current density. Since the storage regeneration process has been eliminated, the deflection systems now required long-term stability as well as short-term stability.

The Selectron was in many respects just like the holding gun tube except that each cell had, in effect, its own electron gun and the method of interrogation was different. This tube compares quite favorably with the other forms of electrostatic storage but when these are compared with magnetic core storage, the cores are preferred. All the electrostatic storage forms have the disadvantage that 1's are read out destructively. In all of these tubes the reading, writing, and sensing of information relies on some sophisticated pulsing techniques of the electron guns and backing plates.

Delay line storage (mercury, quartz, magnetostrictive, and lumped-constant and distribution-constant), capacitor storage, ferroelectric storage and spinecho storage have never been used very extensively for large capacity storage.

Although, for special-purpose application and for small computers not requiring fast access speeds they have been retained.

The present state of the art for other memories is compared in Table 1. This information was extracted from Kosmala, Green and Martin (14). It is evident that beam accessible memories are still the only way of achieving large capacity memories.

B. Statement of the Problem

If a new type large capacity high density memory is to be developed, then some new techniques and/or materials must be found. The major problem with many memories is that the number of wires needed becomes unmanageable. For small computers the wires problem is tolerated but for large capacity systems the computer industry has been devoting monies to the development of methods that eliminate this problem. For example, the use of laser beams for interrogating a memory cell requires only the laser power supply leads, the x-y deflection leads, and the light collector output leads. Which is only 9 leads! Electron beams and lasers are the only methods for use to date that allow the sensing to be accomplished at high speeds. Other systems have large inertia and do not permit totally random access. Magnetic drums and tapes are prime examples.

Table 1. Capacity of computer memories

Memory Material	Packing Density
Ferrite Cores	1000-3000 bits/sq. in. If requirements for very high speed were reduced then densities in excess of 50,000 bits/cu. in. should be realized
Planar Ferrite or laminated ferrites	2000-4000 bits/sq. in.
Planar Thin Film	
a) Split film	800 bits/sq. in.
b) Mated film	200 bits/sq. in.
c) Coupled film	10^4 bits/sq. in.
d) Post-and-film	2000 bits/sq. in.
Plated Wire	500-1000 bits/sq. in.
Serial, block oriented magnetic sonically scanned	10^4 bits/cu. in.
Semiconductor - MNOS metal-nitride-oxide-semiconductor	10^6 bits/cu. in.
Beam Accessed	
a) Photographic (silver halide)	$>10^9$ bits/sq. in.
b) Vaporization (Bi)	$6x10^8$ bits/sq. in.
c) Photochromic ($SrTiO_3$)	$>10^9$ bits/sq. in.
d) Ferroelectric ($LiNbO_3$)	$1.5x10^9$ bits/sq. in.
e) Magnetooptic Curie point (MnBi)	$>6x10^8$ bits/sq. in.
f) Thermoplastic	not available
g) Photoconductive	not available
Cryogenic	$>10^4$ bits/sq. in.

Long-term and short-term stability are two problems that require a controlled environment to minimize data losses. For the magnetic devices temperature, humidity, and stray electromagnetic fields must be properly controlled. The electronics for the deflection systems as well as the deflecting media for lasers are highly temperature sensitive. If, for example, an electron beam was deflected over a 5 inch screen by using 500 volts, then the voltage change required to move the beam would be 3.95 millivolts/micron. If the memory cells are located on 5 micron centers which leads to a 2.5×10^6 bits/cm^2 density and if information is lost by beam displacement of 1.5 microns or 5.925 millivolts, then the acceptable drift of the power supply would be limited to at most 12 parts in a million. If the other direction is included (both x and y drift), then the limit would be down to 8 parts in a million. Consequently, the deflection power supplies would have to be very highly regulated. A common technique to enhance the reliability is to provide redundancy by using several cells to record a bit. The problems of stability and reliability are standard for large capacity memories and require no further discussion.

The decision then is to use an electron beam accessed memory. The fundamental principle to be employed in this memory is the bistable resistivity phenomena that occurs in nonoxide IVA-VA-VIA chalcogenide glasses. This material meets

the memory criteria:

1. The memory elements must have two stable states.
2. These states must be easily and quickly switchable.
3. They must be switchable by an electric field or by heating because these are the two primary effects that an electron beam produces when interacting with matter.
4. These states must exhibit some change that can be sensed with an electron beam.

Both Sie (26) and Uttecht, Stevenson, Sie, Griener, and Raghavan (29) have demonstrated the memory bistable resistivity of As-Te-Ge. This provides evidence for the satisfaction of the first three memory criteria. The only condition left to be satisfied is the fourth one of electron beam sensing.

To sense with an electron beam it is desirable to find a material that has a large secondary electron emission change for a given electron beam energy when switching from one state to the other. This notion has served as a primary motivation for the work in this thesis.

C. Method of Attack

The As-Te-Ge chalcogenide glass was selected from the non-oxide IVA-VA-VIA chalcogenide glasses because of the availability of information about its physical properties. The

ternary system of As-Te-Ge is shown in Figure 1 which was reported by Hilton, Jones and Brau (11) and Krebs and Fischer (15). Also this system provides two glass regions that exhibit different switching phenomena. The glass island in the lower left hand corner of Figure 1 is used to make threshold switching devices. The other glass region is used to make memory switching devices.

The difference between the two types of devices is that the threshold device will only remain switched as long as there is enough voltage and current applied so that the conducting filament state can be maintained. The memory device differs because it will remain in a state until there is some impetus applied to cause a change of state.

This glass system abounds with information about most of its physical properties (11, 12, 15, 22, 26, 29, 30, 31). As a consequence, the main effort of the work is directed towards measuring the secondary electron characteristics and not in measuring the resistivities, densities, thermal expansion coefficients, glass transition temperatures, etc.

There are numerous different ways that the secondary electron characteristics can be measured. The advantages and disadvantages of each is described by Whetten (32). The method that was chosen to make these measurements is the two electron gun technique that was developed by Handel, Jensen, and Siedband (10). This technique provides a steady state

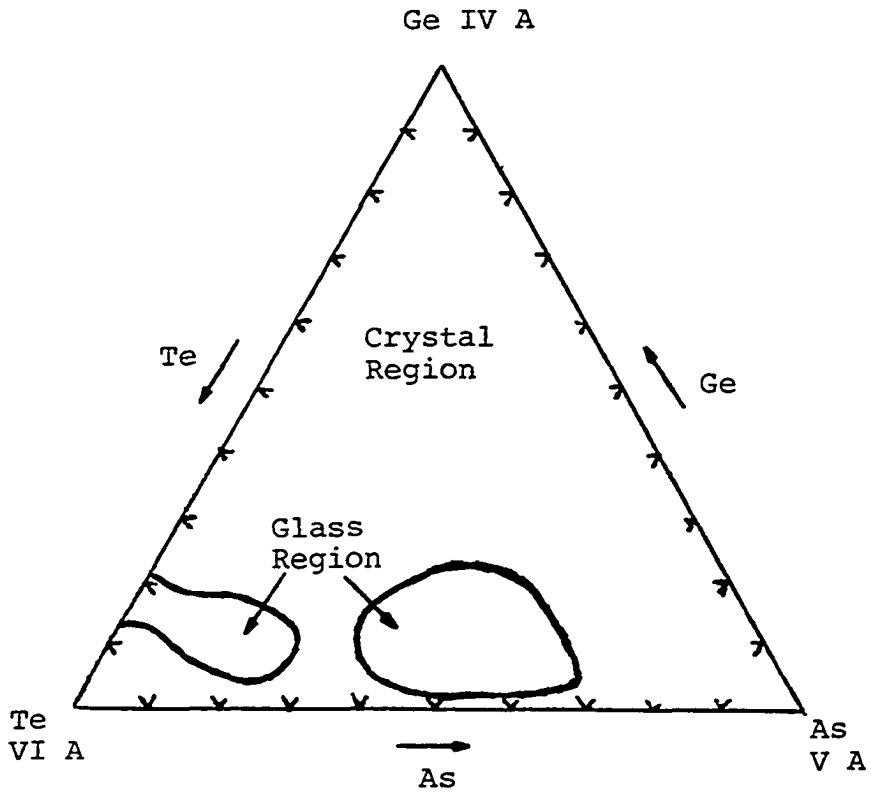

Figure 1. The As-Te-Ge phase diagram in atomic percentage (after Hilton)

measurement of the secondary electron emission characteristics.

Figure 2 shows the current relationship that exists at the target. The reflected current consists of true secondaries, elastically scattered primaries, inelastically scattered primaries, Auger electrons etc. For current balance at the target the following relationship must be satisfied:

$$I_{primary} = I_{reflected} + I_{transmitted}$$

Dividing this equation by $I_{primary}$ and moving the third term to left side of the equation gives

$$\frac{I_{reflected}}{I_{primary}} = 1 - \frac{I_{transmitted}}{I_{primary}} .$$

But the secondary emission ratio is defined as

$$\delta = \frac{I_{reflected}}{I_{primary}} .$$

It follows then that

$$\delta = 1 - \frac{I_{transmitted}}{I_{primary}} .$$

In order to measure δ the primary and the transmitted currents need to be measured. These can be measured quite handily by this technique as compared to the relatively difficult pulsing techniques. Figure 3 is a schematic of the secondary electron emission analyzer. A full description of the operation of this analyzer is deferred until a later section.

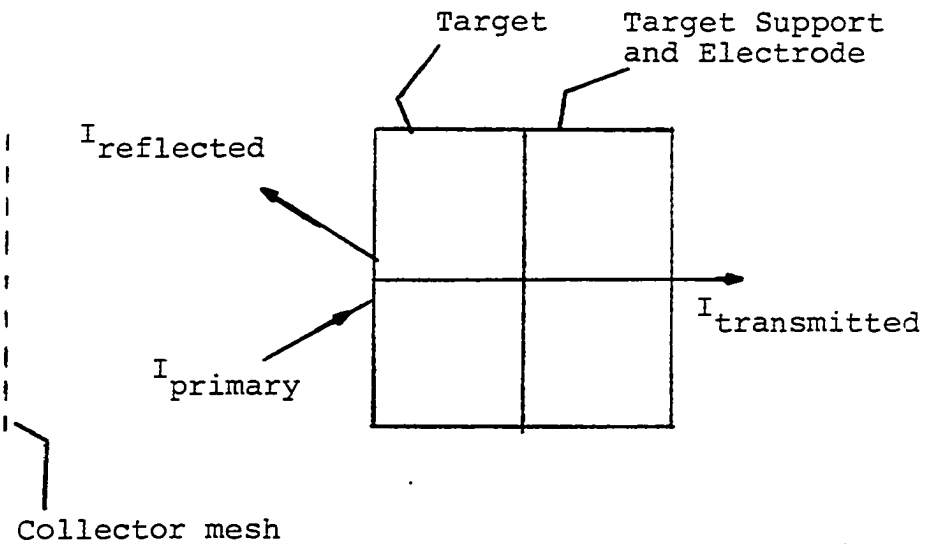

$$I_{primary} = I_{reflected} + I_{transmitted}$$

Figure 2. Current relationship at the target

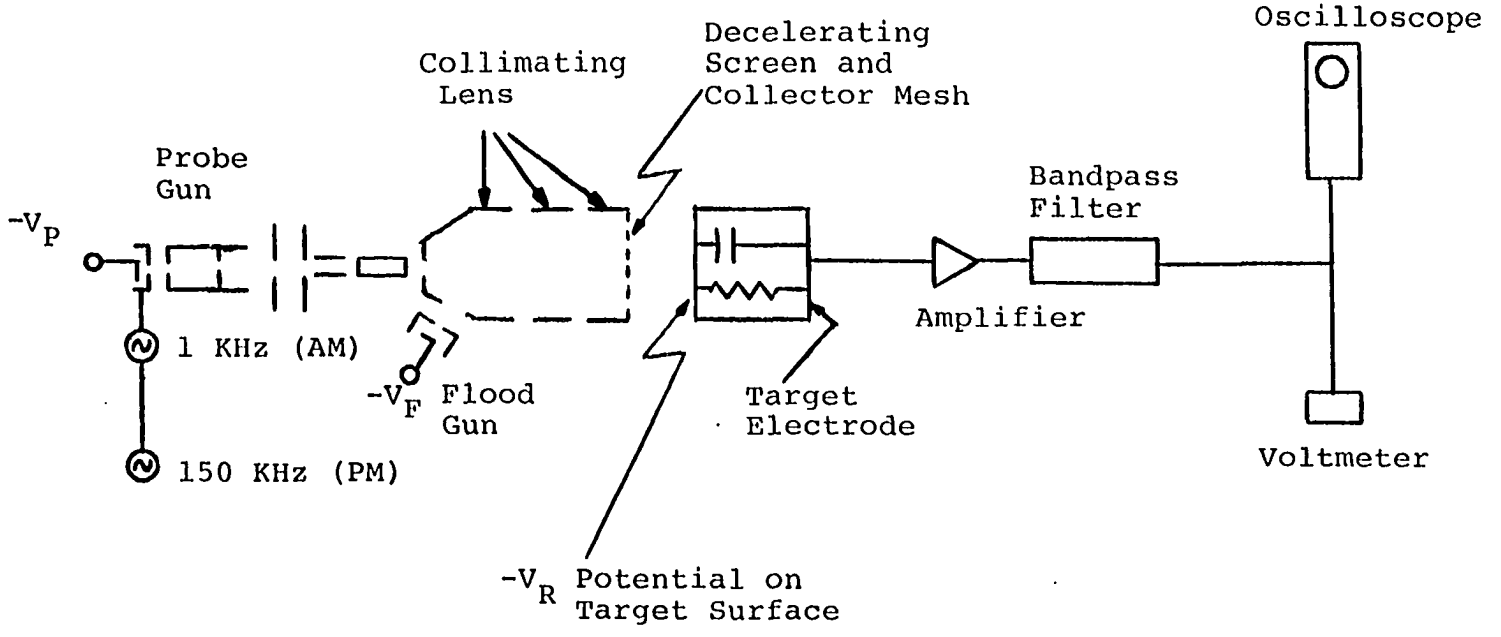

Figure 3. Schematic of the secondary electron emission analyzer

The salient features of the technique are that the flood gun holds the surface of the target at a constant potential while the probe gun is modulated by a 1 kHz source. The transmitted current consists of a dc current plus an ac current. The ac current is amplified, run through a band-pass filter, and then the signal is measured with an oscilloscope. To measure the primary current the target is simply replaced by a Faraday Cage.

II. LITERATURE REVIEW

In 1902 Austin and Starke discovered the phenomenon of secondary electron emission. They were studying the reflection of cathode rays from metallic surfaces when they found that the metal surfaces were emitting more electrons than they were receiving. If it had been pure reflection, then the number incident would have been equal to the number reflected but this was not the case. Consequently, it provided positive proof of the liberation of electrons from the material itself.

When electrically charged particles of sufficient kinetic energy strike a material, the material will emit electrons. The incident particles can be electrons, ions, protons, etc. Only incident electrons will be considered and these will be called the primary electrons. When these primary electrons bombard a material, the electrons are slowed down through energy losses due to the interactions with the atomic forces of the material. Some of this energy will produce excitation of electrons in the material. These electrons will diffuse throughout the material and if they reach the surface, they may escape through the surface barrier. These electrons are referred to as the secondary electrons. For thin slabs secondary electrons will be emitted from both surfaces but the ones that are normally considered are the ones that emerge from the side being bombarded by the primary electrons. Figure 4 shows the relationships between the primary, secondary

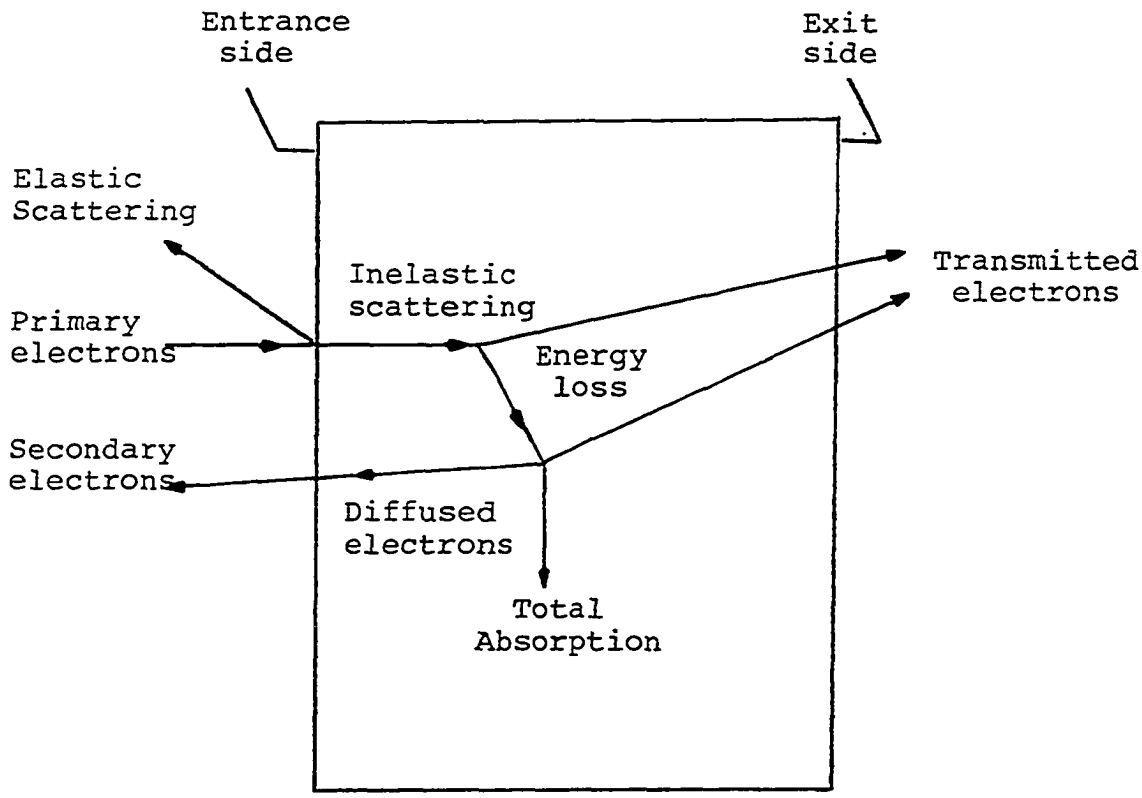

Figure 4. Origin of secondary electrons

and transmitted electrons.

Interaction within the slab does not necessitate the release of electrons. The electrons emerging from the entrance side will consist of inelastically scattered primaries, elastically scattered primaries, Auger electrons, true secondaries, and other competing processes of energy absorption leading directly or indirectly to excited electrons. An energy spectrum of the emitted electrons is shown in Figure 5 from Rudberg (23). The peaks in the spectrum are distinguishable and are termed:

a. Elastically reflected primaries

b. Inelastically reflected primaries

c. "True" secondaries

The broad peak (c) contains the majority of the emitted electrons. The energy distribution of these slow electrons is practically independent of the primary electron energy. Consequently, these electrons are referred to as the true secondaries. On the other hand, it is impossible to separate the true secondaries from the inelastically scattered primaries. Arbitrarily, the term "true" secondaries refers to all those electrons below an energy of 50 eV.

Experimentally, it is easier to measure the total number of reflected electrons and in most applications the gross effect is utilized. In the literature the δ described refers to the ratio of the total emitted secondary electron current

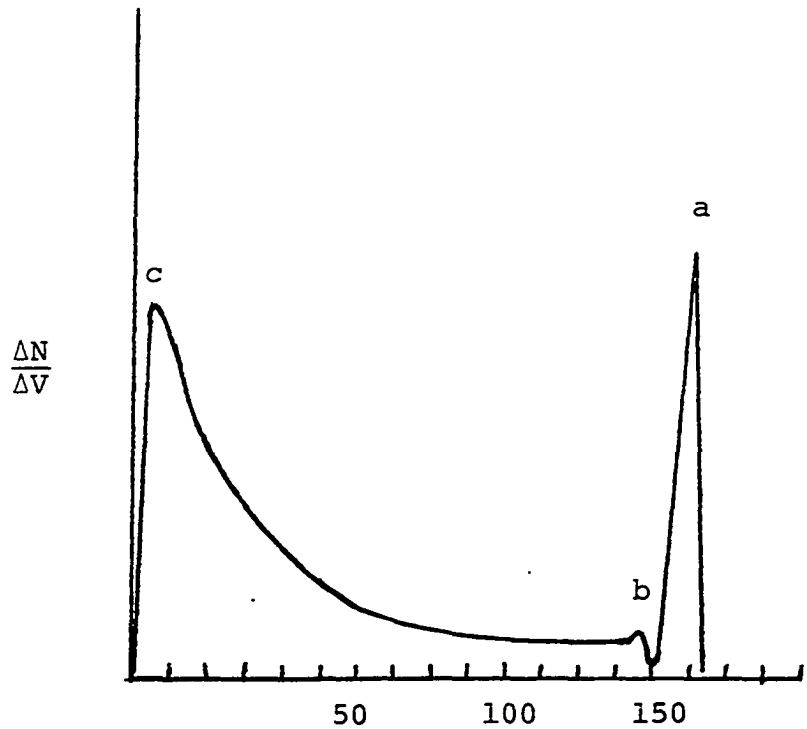

Figure 5. Distribution in energy of secondary electrons from gold for a primary electron energy of 155 eV (after Rudberg)

to the primary electron current.

There have been a number of theoretical treatments of the phenomenon of secondary electron emission (3, 7, 8, 25). As yet, however, it is impossible to predict in detail the secondary emission characteristics of a material from its fundamantal properties.

The yield of a material is dependent on the energy of the primary electrons, the angle of incidence of the primaries with respect to the surface, the properties of the surface being bombarded, and the properties of the bulk material. The surface conditions highly affect the number of secondary electrons. Therefore, its past history must be well-known in order to make the results meaningful.

Measuring δ for metals is much easier than it is for insulators. Insulators are difficult because surface charge accumulations affect the measurements. The insulators will remain at the same potential only when $\delta = 1$. In order to make any measurements of δ, the charging of the surface must either be eliminated or at least minimized.

The heating of some insulators will increase the conductivity sufficiently so that there will not be much charge accumulation. The problem with this technique is that δ is temperature dependent due to increased scattering between electrons and lattice vibrations as shown by Dekker (7).

Pulse methods are used to keep the charge accumulation

small and are the most versatile methods developed to date. These methods reduce charging by reducing the number of incident electrons. After a pulse the surface potential is re-established by one of the following:

1. If the insulator is a thin film on a conducting substrate, electrical leakage or breakdown through the insulator, thereby, keeping the surface potential near the substrate potential.
2. Heating of the insulator but allowing adequate cooling time.
3. Flooding the surface with low-energy electrons and causing the surface to be at the potential of the filament.
4. Using secondary electron emission to re-establish the surface potential.

Each method has a few good and bad qualities so the experiment will have to dictate the choice. Method 2 appears to be the best but is extremely time-consuming.

There are two standard ways to measure δ. They both involve using a target located in the center of a spherical collector and a grid spaced slightly inside the collector. The collector geometry and collector potential is such that it collects all of the electrons coming from the target. The grid is used to repel the secondaries liberated from the collector due to the collecting of electrons from the target.

In method 1 the collector current is measured and the target current is measured. The sum of these two is the primary current. Method 2 uses the target circuit to make both measurements. After the target current is measured the collector is made negative to repel the target emitted electrons so that they are all recollected by the target. The only problem here is that if there are any target emitted electrons of sufficient energy to reach the collector, then this component will not be measured. Also, the secondaries from the collector due to this current will be accelerated to the target and give a false addition to the primary current. The advantage of this method is that the target circuitry is used for both measurements. This means that the input capacity to the preamplifier is the same in both measurements. δ is the ratio of two currents so the amplifier need not be calibrated in terms of current to the amplifier. For a more detailed discussion of these techniques see Whetten (32).

Three papers (4, 17, 18) have been published on the measured secondary emission characteristics of nonoxide IV-V-VI chalcogenide glasses. All three used pulse techniques similar to those already discussed. Makedonskii and Pustovoit (17) and Makedonskiy (18) dealt strictly with binary compositions and did not with one exception make a comparison of the characteristics for sample compositions prepared in both the amorphous and the crystalline state. Consequently, their re-

sults were not very exciting.

The work of Chen, Norton and Wang (5) did present results for two samples of As-Te-Ge in the amorphous and the crystalline phases. They also presented data for one composition as a function of annealing temperatures between 23°C and 520°C. For the composition $Ge_{4.8}As_{17.2}Te_{78}$ the δ_{max} was 1.95 for the amorphous state versus 1.20 for the crystalline state. This looks very promising.

III. EXPERIMENTAL

A. Secondary Electron Emission Analyzer

The secondary electron emission analyzer is patterned after the method developed by Handel et al. (10). The schematic for this analyzer is shown in Figure 6. This method uses two electron guns and these are denoted the probe gun and the flood gun. The flood gun is used to hold the front surface of the target at a fixed potential. The probe gun is used to interrogate the surface. The collimating lens mixes the two beams and bends the flood gun beam since the flood gun is located off axis. The transmitted signal is amplified, run through a bandpass filter and then monitored with an oscilloscope and an rms voltmeter.

The secondary emission coefficient δ is measured in the following way. The charge balance equation for the currents at the target is:

$$I_{primary} = I_{secondary} + I_{transmitted} .$$

Dividing this equation by $I_{primary}$ and rearranging:

$$\delta = 1 - \frac{I_{transmitted}}{I_{primary}} .$$

Note, that this is the gross effect secondary emission coefficient. If the primary and the transmitted currents are measured, then it is easy to compute δ.

Figures 7 and 8 are pictures of the analyzer. The

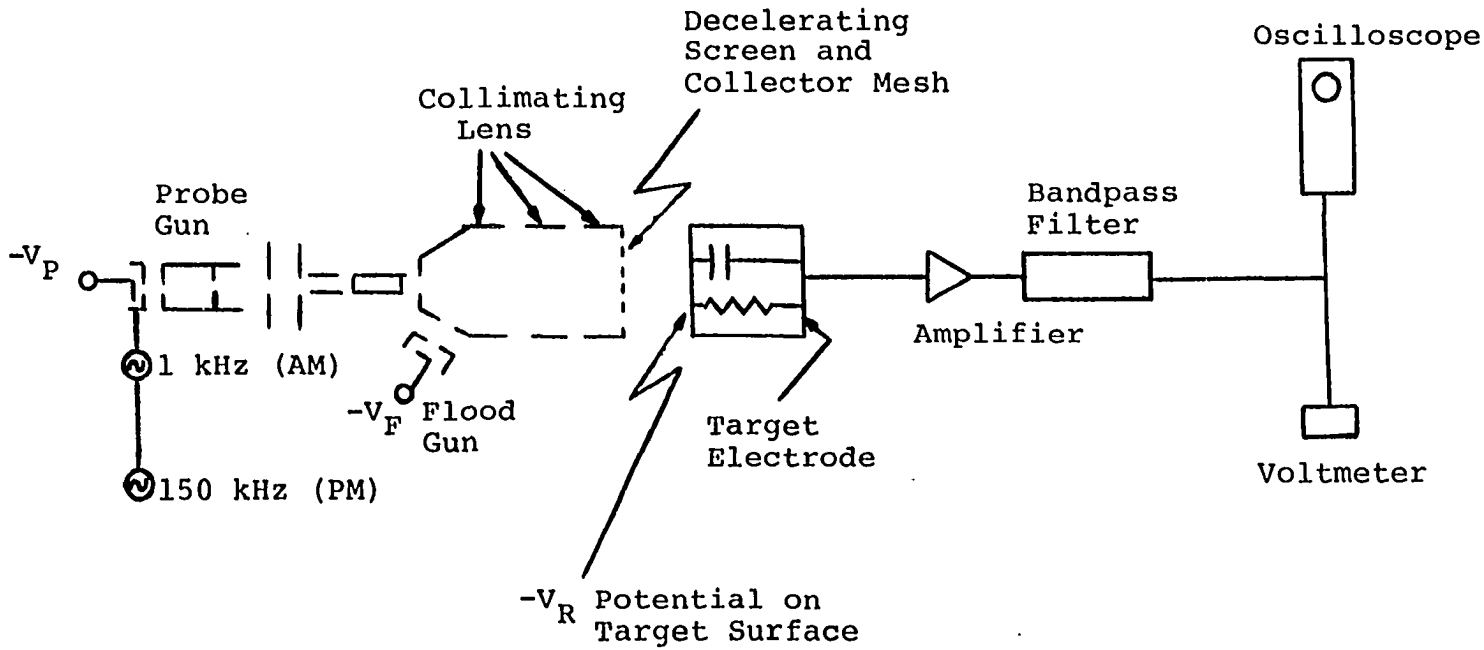

Figure 6. Schematic of the secondary electron emission analyzer

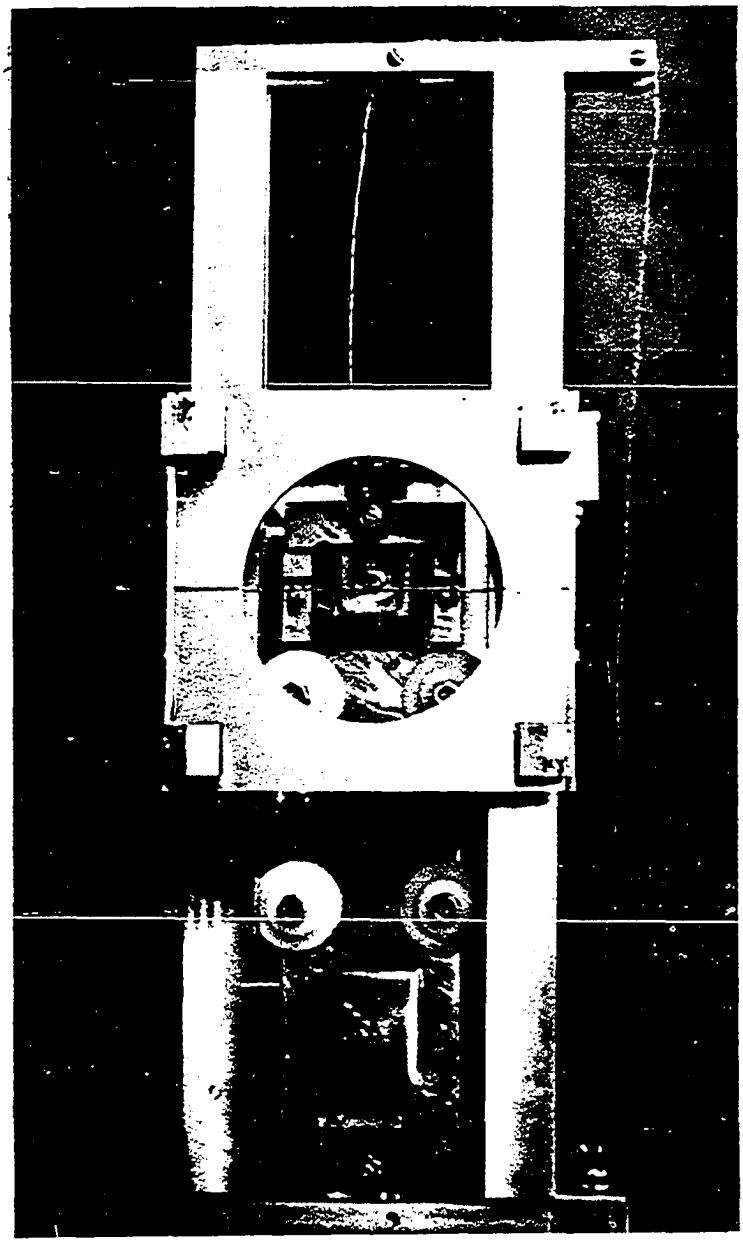

Figure 7. Target support plate, target holders and the Faraday Cage of the secondary electron emission analyzer

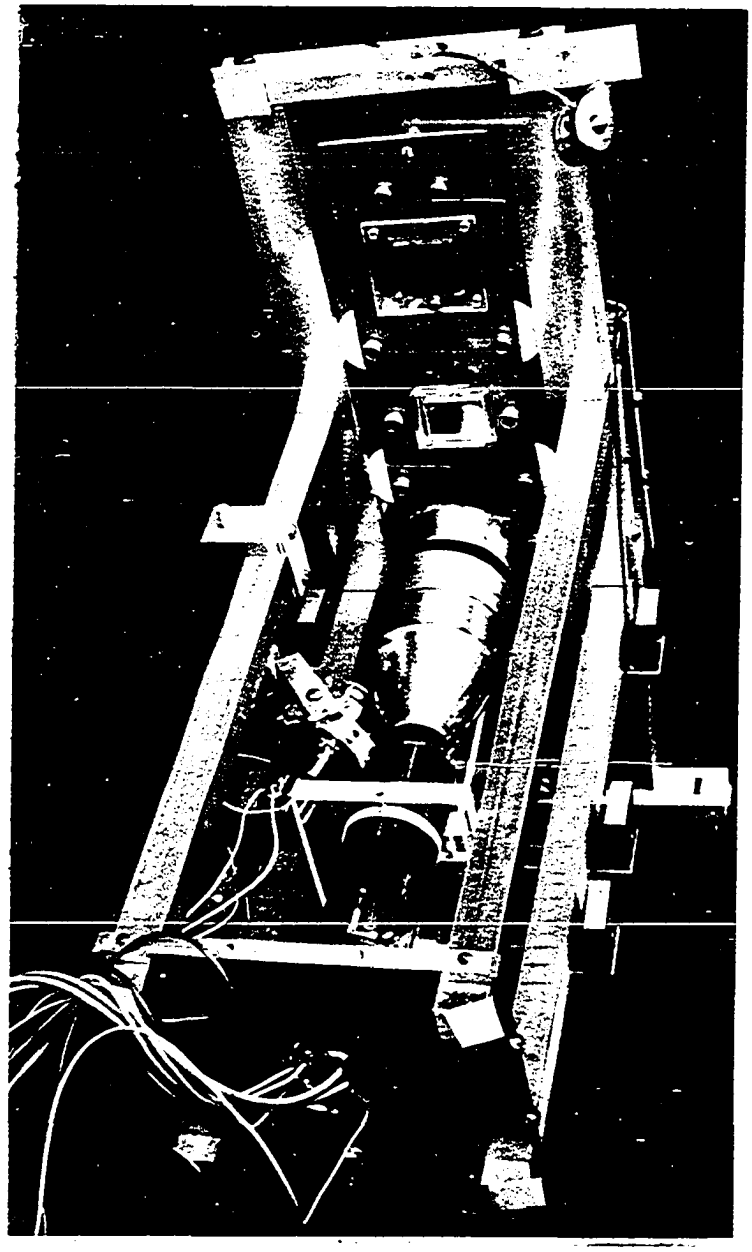

Figure 8. The probe gun, the flood gun, the collimating lens, and support structure for the secondary electron emission analyzer

analyzer was constructed in the following manner. The four guide rails were made of aluminum 3/4" x 3/4" x 17". The two end support plates were fashioned from aluminum 6" x 6" x 3/8". The gun and collimating lens were fashioned out of aluminum and plexiglas. The target support plate guides were also fashioned from aluminum. The target support plate guides were made of nylon and the plate itself was fabricated from inconel. The target holders and the Faraday Cage holder and positioner were made from plexiglas. The Faraday Cage and the collimating lens were constructed of stainless steel. Picture hanging cable was used to raise and lower the target support plate. The materials were selected on the basis of being nonmagnetic, nonreactive, good insulators (if need be), of good vacuum characteristics, and easily machinable (except inconel).

The probe gun was an old World War II vintage 5BP1 cathode ray tube. The vacuum was released in the tube and then the tube was severed at the deflection plates. The probe gun deflection system was operated in parallel with a Dumont 341 oscilloscope. This permitted a constant check on the beam position. A high voltage power supply was utilized to obtain voltages between 0 and 4600 volts.

The flood gun was constructed by modifying a 5FP7 cathode ray tube. This consisted of removing the gun from the glass envelope and then cutting off everything above the cathode.

The cathode and filament were tied together. The filament voltage was provided by a dc supply and the cathode potential was provided by a tap from the voltage network used for the collimating lens.

The collimating lens consists of three stainless steel sections. The first one was constructed with a truncated cone and a right circular cylinder. The probe gun aperture was a one-half inch opening located on axis at the center of the truncated cone. The flood gun aperture was made by cutting away part of the right circular cylinder and the truncated cone and was located approximately 15° off axis. The second section was a right circular cylinder and the third was too, except that a 50 mesh stainless steel screen was welded to the face nearest the target. A voltage divider network was used for the lens with the third section at 390 volts, the second at 260 volts, and the first at 130 volts.

A phosphor screen was located on the target support plate and was used to locate the beam and to study its shape and intensity. The phosphor screen was made in the following manner. A plate of glass was cleaned in a 10% solution of hydrofluoric acid and then rinsed with distilled water. After drying, the plate was coated with a weak phosphoric acid solution and carefully sprayed with zinc sulfide, an electronic phosphor. It was then placed in an oven, heated to 400°C, the oven turned off, and then extracted the next day. This method

provided a very durable screen. This screen was later removed so that two samples could be analyzed.

The Faraday Cage consists of a 3/4" x 3/4" x 1" stainless steel box with a 1" x 1" x 1/2" snout on it. The inside was coated with soot from an enriched acetylene flame. This was done to decrease the number of secondary electrons emitted during the collecting process. δ_{max} for soot is a low 0.45 and this occurs at an incident electron energy of 500 volts (32). The orifice of the Faraday Cage was equal in size to that exposed by the targets. Hence, the beam impinging on the targets was identical to that entering the Faraday Cage.

The analyzer is located in a stainless steel bell jar that is 18 inches in diameter and 24 inches tall. High vacuum feedthroughs are used for all connections and in the case of the collimating lens and the probe gun heater leads, the feedthroughs are high voltage, as well. The system is pumped by a 6 inch diffusion pump using DC-704 oil. This equipment is shown in Figure 9.

The signals produced by the samples and the Faraday Cage are fed through 50 ohm coaxial cables. The signals are amplified and run through a bandpass filter. The amplifier is a modification of the circuit from Miller (19) and the bandpass filter is a Krohn-Hite Model 3100. The output is monitored on a Tektronix 561A dual beam oscilloscope and a Ballantine

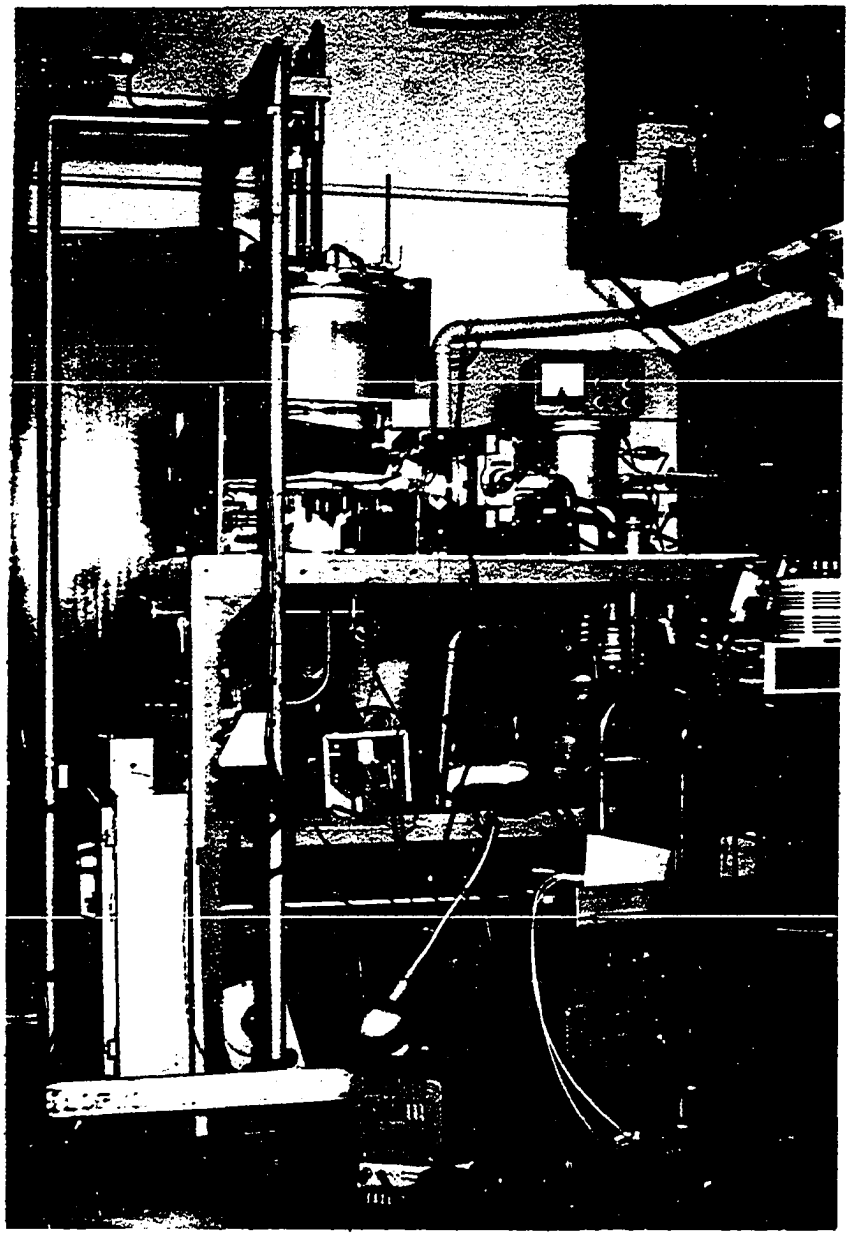

Figure 9. The vacuum and electrical equipment for the secondary electron emission analyzer

Model 300 electronic voltmeter. Modulation of a 250 x 10^{-12} A probe beam current produces the output signal. A Hewlett Packard Model 200CD widerange oscillator and a Hewlett Packard Model 211A square wave generator are used to pulse amplitude modulate the probe beam. Another oscillator is used to swing the probe beam in a circular fashion on the targets. This, in effect, provides an infinite number of samples from one sample simply by changing the shape of the probe beam. The probe beam for the higher voltages is approximately 1 mm in diameter.

The transmitted current and the primary current are easily measured. The target support plate is moved vertically and an optical alignment is used to correctly position the plate. Although, this method is very time consuming, the beam distortion that occurs when bending the beam to deflect it to either the target or the Faraday Cage would produce questionable results. In particular, for low voltages, the distortion would be quite large.

When insulators are analyzed, the flood gun cathode is clamped at zero volts. If the surface starts to charge positive, more electrons will be drawn from the flood gun. In the case of semiconductors, a potential difference due to an IR drop through the material, can cause errors in computing the primary electron energy and thus errors in δ. This problem is alleviated by adjusting the flood gun cathode to a negative

potential relative to the grounded target electrode (neglecting the IR drop across the amplifier input resistance). This will establish a surface potential close to that of the flood gun cathode. Also, the potential is held constant throughout the experiment.

This technique is only good for measuring the characteristics between first and second crossover. The reason is that since this is a steady state measurement there will be a net negative charge accumulation for $\delta < 1$ which will drastically affect the number and energy of the impinging probe beam. The surface potential would not be a constant during the measurement.

The probe beam current should be a small perturbation, which means that the average current density of the probe beam must be much less than the flood beam. This can be accomplished by using a small probe beam current, by pulse amplitude modulating the probe beam, and by scanning the probe beam to keep the duty cycle small on a particular area of the target.

B. Calibration Samples

The calibration sample is selected on the basis that since glasses are to be analyzed the calibrator should be a similar but a well-known material. Quartz was selected and its characteristics were published by Salow (24) and Geyer (9).

The sample substrates are 30 mil thick 1-1/8" x 1-1/4" stainless steel plates that have a small tab silver soldered to the center of the back side. The surface is polished in the following steps:

1. Hand polished with 240 grit silicon carbide paper
2. Hand polished with 600 grit silicon carbide paper
3. Hand polished with a nylon cloth and 1 micron sized alumina calcined powder in a slurry
4. Hand polished with a nylon cloth and 0.05 micron sized alumina calcined powder in a slurry
5. Hand polished with a microcloth and 0.05 micron sized alumina calcined powder in a paste

After this polishing of about one and one-half hours per substrate, the substrates are washed with distilled water, acetone and then alcohol. They are then placed in an ultrasonic cleaner for one-half hour. The cleaner contained a solution of distilled water and a detergent. Finally, they are placed in an alcohol degreaser for 12 hours. In order to further the smoothing, a 1000 angstrom layer of chromium is deposited.

The quartz is deposited by an rf sputtering technique. The film thickness is 5500 angstroms. This thickness is used because the electron beam would not be able to penetrate to the substrate and any thicker layer would have involved some complications with the deposition technique.

The secondary electron emission characteristics for quartz are shown in Figure 10. The clean sample is a virgin sputtered film. The disagreement with Salow (24) for this clean sample

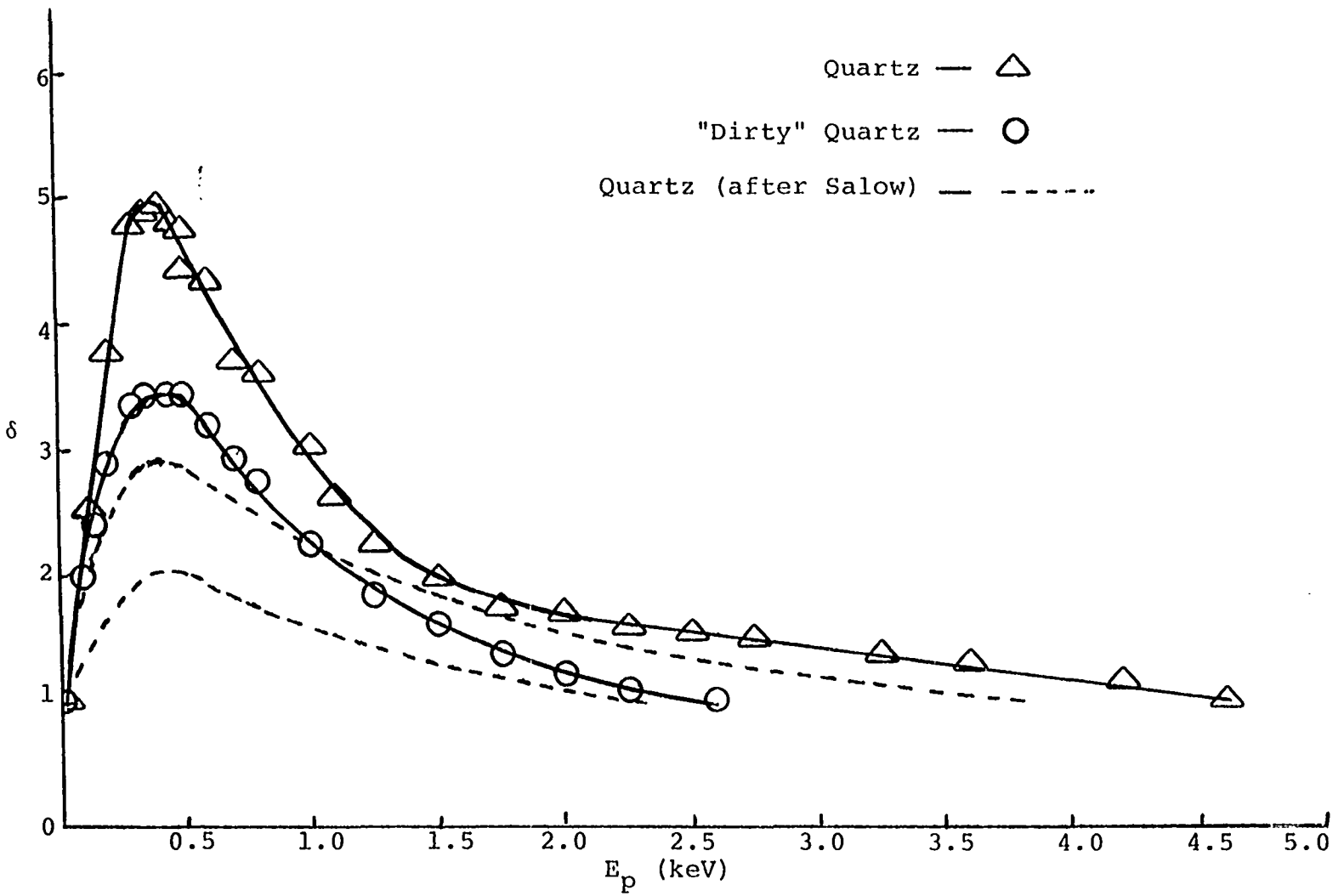

Figure 10. Secondary yield of quartz samples

is thought to be based upon the method of sample cleanliness. Salow's samples were prepared by acid etching and washing with distilled water. A "dirty" sample was prepared by etching with nitric acid and then hydrochloric acid, washing with isopropanol and distilled water. Much better agreement is obtained as shown in Figure 10.

C. Chalcogenide Glass Samples

The chalcogenide samples are made by weighing out the percentage atomic weight of each element. They are then mixed together in quartz ampules. A vacuum is drawn and then the tubes are sealed. Some of the ampules are placed in 304 stainless steel cylinders and packed with carbon cloth to prevent breakage. The cylinders are sealed in a helium environment. The stainless steel cylinders and the remaining quartz ampules are then placed in a rocking furnace and rocked for 24 hours after reaching the 980-1020°C temperature range. After removal from the furnace, part of the samples are plunged into water at room temperature and the rest are air cooled to room temperature.

The sample substrates are prepared in the same identical manner that was used in the preparation of the substrates for the calibration samples. The chalcogenide glass is then deposited onto the substrates by electron beam evaporation. Figure 11 shows the arrangement for performing this deposition.

Figure 11. Electron beam evaporator for the deposition of chalcogenide glasses

The substrate holder is loaded with two stainless steel substrates, ten circular cover glasses 22 mm in diameter, four silicon wafers 1" x 1" or less and one quartz crystal. The substrates are cleaned with a detergent soap and distilled water solution in an ultrasonic cleaner for 30 minutes followed by 12 hours in an alcohol degreaser. After placement into the evaporator, the system is pulled down to at least 2×10^{-5} mm and then a 200 watt heater is turned on for two hours. Then after a 24 hour cooling period, the deposition is performed at a pressure of less than 5×10^{-6} mm.

The glass samples are switched by the following method. A 38 mm inside diameter pyrex tube is attached to a vacuum valve as shown in Figure 12. An aluminum boat is fabricated by machining a halved aluminum rod, anodizing it and then boiling it in water. The boat holds the targets, glass samples and bulk material. The tube is loaded and then pulled down with a mechanical pump. The tube is sealed off and then placed in a tube furnace that has been preheated to 440°C. The furnace is switched off such that the boat is heated to 350°C for 3 minutes and then cooled at a 2°C per minute rate. After cooling to 100°C the tube is reattached to the mechanical pump, the vacuum valve opened and left in this condition until the analyzer is ready to measure its characteristics.

The composition is determined by microprobe analysis, the thickness by interferometer, and the resistivity ratio by a

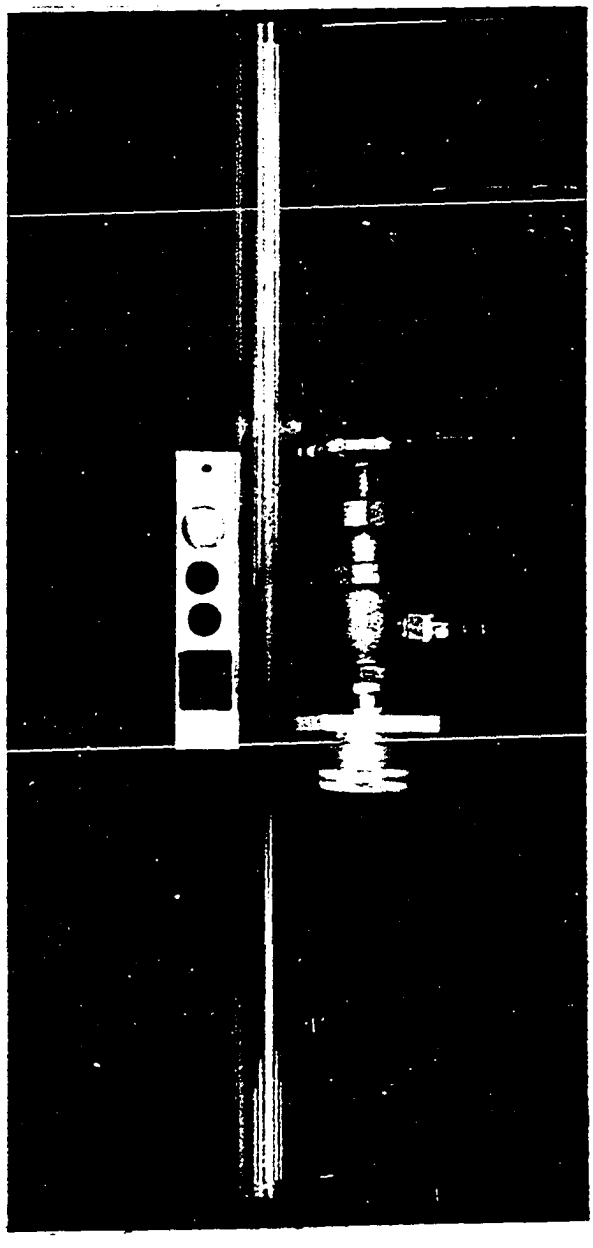

Figure 12. Pyrex tube, loaded boat and vacuum valve used for switching the chalcogenide samples

four probe technique (16). These measurements are made on the glass substrates that accompanied each deposition and not on the stainless steel substrates. The four probe technique is used in the square-probe array. The sheet resistance is then found to be

$$R_s = 9.06\ V/I$$

where

R_s = sheet resistance

V = potential between two adjacent probes

I = current flowing through the other two probes.

Resistivity is then found by $\rho = R_s d$, where d is the film thickness. Probes with 5 mil diameter points are used and they have a tendency to poke a hole in the film. Extreme care must be used to prevent this. These results are also compared to a two probe dc technique and found to be in agreement. Some of the films on both the glass and stainless steel substrates were compared and found to be in agreement also.

The sample compositions were selected on the basis of investigating the memory switching region. The vapor pressure difference of the three elements resulted in compositions that are somewhat different from the bulk material. This is discussed in more detail in the discussion section.

D. Results

The microprobe analysis is presented in Table 2. The deposition 110 was analyzed to determine if the deposition method produced a uniform composition over the surface of the substrate holder. Four of the ten cover glasses were randomly selected and analyzed. The results are well within the 10% accuracy of the microprobe analyzer. The two glass samples that were switched with this sample turned out defective in that one completely peeled and the other partially peeled so that no good microprobe results could be obtained. The only other malfunction is the sample G. Upon switching the glass, it peeled off of the stainless steel substrates. The surfaces must not have been clean enough in order for this to have occurred. There is a difference between the amorphous composition and the crystalline but almost all of them are within the region of overlap when the microprobe error is included. The crystalline compositions will be used to denote the sample composition when reference is made to it. The compositions are plotted in Figure 13.

The resistivities are listed in Table 2. These values are in agreement with those reported by Hilton et al. (11). The resistivity ratio varied from 2×10^4 to 1×10^7.

The secondary electron emission characteristics were determined with the secondary electron emission analyzer operating under the following typical conditions:

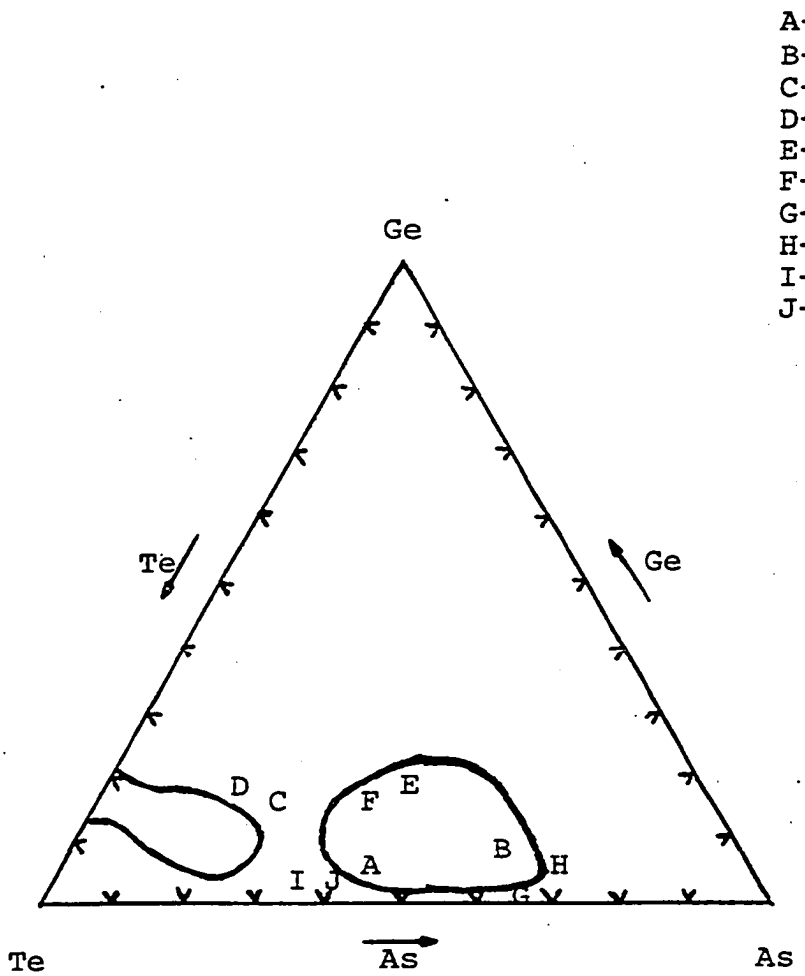

Figure 13. Diagram of the samples analyzed

Table 2. Sample composition and resistivity

Sample	Sample Number	State	Composition %Ge	%As	%Te	Resistivity Ω-cm
A	100	Amor.	4	41.6	54.4	2×10^{3}
	101	Crystal.	4.1	47.3	48.6	1×10^{-1}
B	110	Amor.	7.4	60.4	32.2	1×10^{5}
	111	Amor.	7	61.3	31.7	
	112	Amor.	6	64.4	29.6	
	113	Amor.	7.8	60.9	31.3	
	115	Crystal.	-	-	-	1×10^{-1}
C	120	Amor.	17	21.9	61.1	2×10^{5}
	121	Crystal.	14.6	27.3	58.1	4×10^{-2}
D	130	Amor.	12.9	23.6	63.5	4×10^{4}
	131	Crystal.	15.3	21.7	63	4×10^{-2}
E	140	Amor.	16.5	41.3	42.2	3×10^{5}
	141	Crystal.	17.9	40.2	41.9	3×10^{-2}
F	150	Amor.	12.8	39.6	47.6	5×10^{5}
	151	Crystal.	15.4	37.8	46.8	9×10^{-2}
G	160	Amor.	0.5	65.1	34.4	4×10^{5}
H	170	Amor.	5.3	72.7	22	4×10^{5}
	171	Crystal.	6.9	67.2	25.9	1×10^{-1}
I	180	Amor.	0.8	35.8	63.4	4×10^{5}
	181	Crystal.	0.8	36.1	63.1	5×10^{-1}
J	190	Amor.	5.6	37.8	56.6	1×10^{5}
	191	Crystal	3.6	42.1	54.3	2×10^{-1}

1. probe beam current of 250 x 10^{-12} A
2. probe beam pulse rate of 150 kHz
3. probe beam amplitude modulation of 1 kHz
4. probe beam sweep rate of 5-20 Hz
5. vacuum less than 8 x 10^{-6} Torr with both guns operating.

The secondary electron emission curves are shown in Figures 14 through 23 and these curves are summarized in Table 3. Note that even though the peak values for some amorphous and crystalline samples are the same, the curves are not. In all cases the two stainless steel samples were well within a few percent of one another and consequently, only one curve is plotted.

Figure 24 shows the microprobe output for crystalline sample C. The surface is highly ordered but the distribution of As, Te, and Ge is completedly random. The Te x-ray output is not shown but is identical to those shown for As and Ge. Figures 24 through 46 show the surface structure for the amorphous and crystalline states of the samples tested. These pictures were taken with a scanning electron microscope. Those prepared on both the glass and the stainless steel substrates were analyzed since the microprobe analysis was performed on the glass and the secondary electron emission was performed on the stainless steel ones. The pictures were selected in that they depicted a typical view of the surface.

Table 3. Secondary yield parameter of quartz and chalcogenide glasses

Sample		δ_{max}	$E_{p\ max}$(V)	E_1(V)[a]	E_2(V)[a]
Quartz	(clean)	4.95	400	25	4600
Quartz	(dirty)	3.45	400	40	2600
A	Amor.	3.62	375	25	4000
	Crystal.	3.62	375	25	4000
B	Amor.	3.20	350	20	3000
	Crystal.	3.52	350	20	4500
C	Amor.	3.30	350	20	3200
	Crystal.	3.72	350	20	3800
D	Amor.	3.40	350	30	3400
	Crystal.	3.40	350	30	3400
E	Amor.	2.68	350	20	2600
	Crystal.	3.25	300	20	3200
F	Amor.	3.50	350	20	3300
	Crystal.	3.77	350	20	3400
G	Amor.	2.57	400	30	3500
H	Amor.	2.85	350	25	3000
	Crystal.	2.95	350	25	3500
I	Amor.	2.92	350	25	3500
	Crystal.	3.25	400	25	4400
J	Amor.	2.82	350	40	3250
	Crystal.	2.97	350	40	4600

[a] E_1(V) and E_2(V) are first and second crossover respectively.

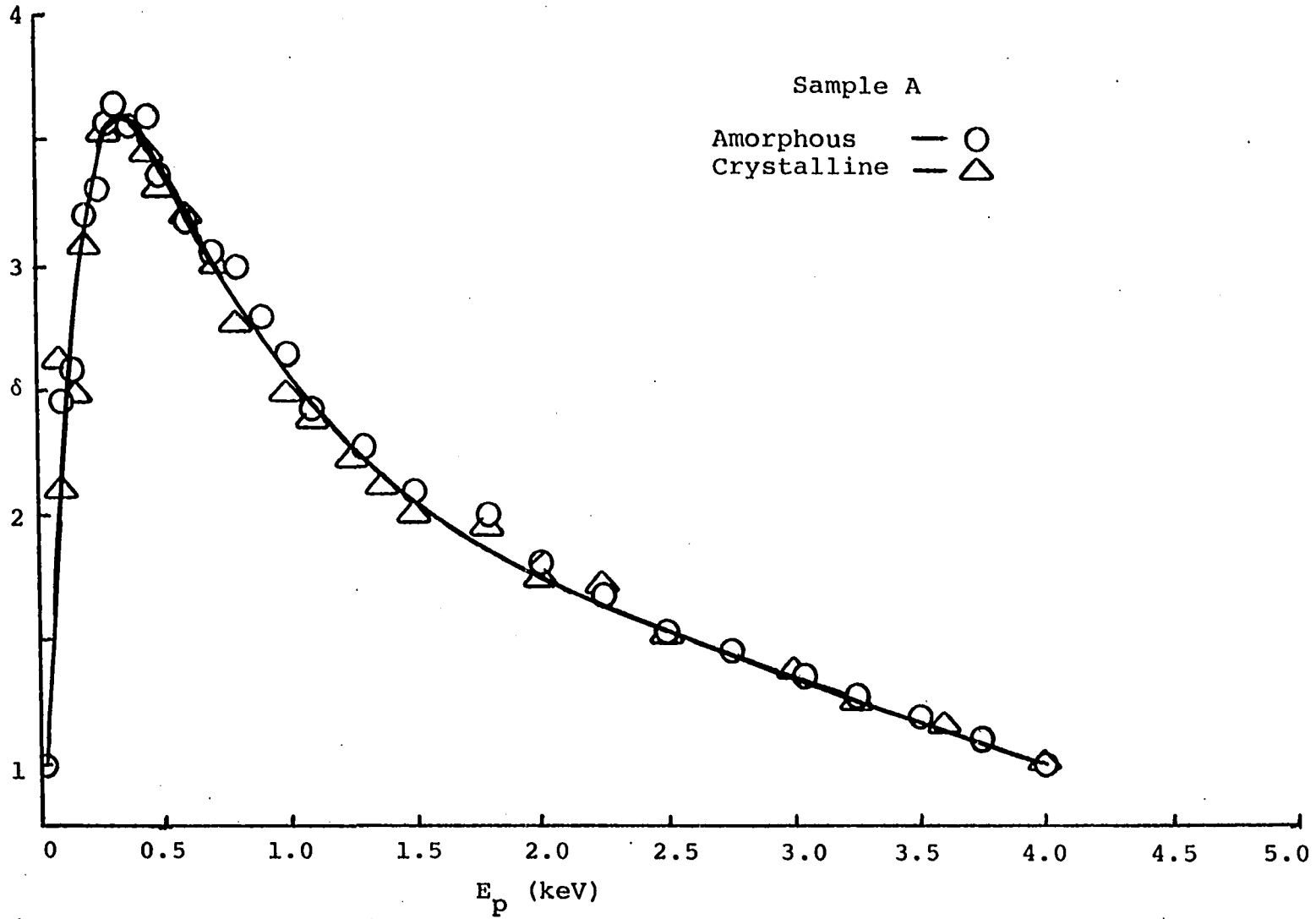

Figure 14. Secondary yield of amorphous and crystalline $Ge_{4.1}As_{47.3}Te_{48.6}$

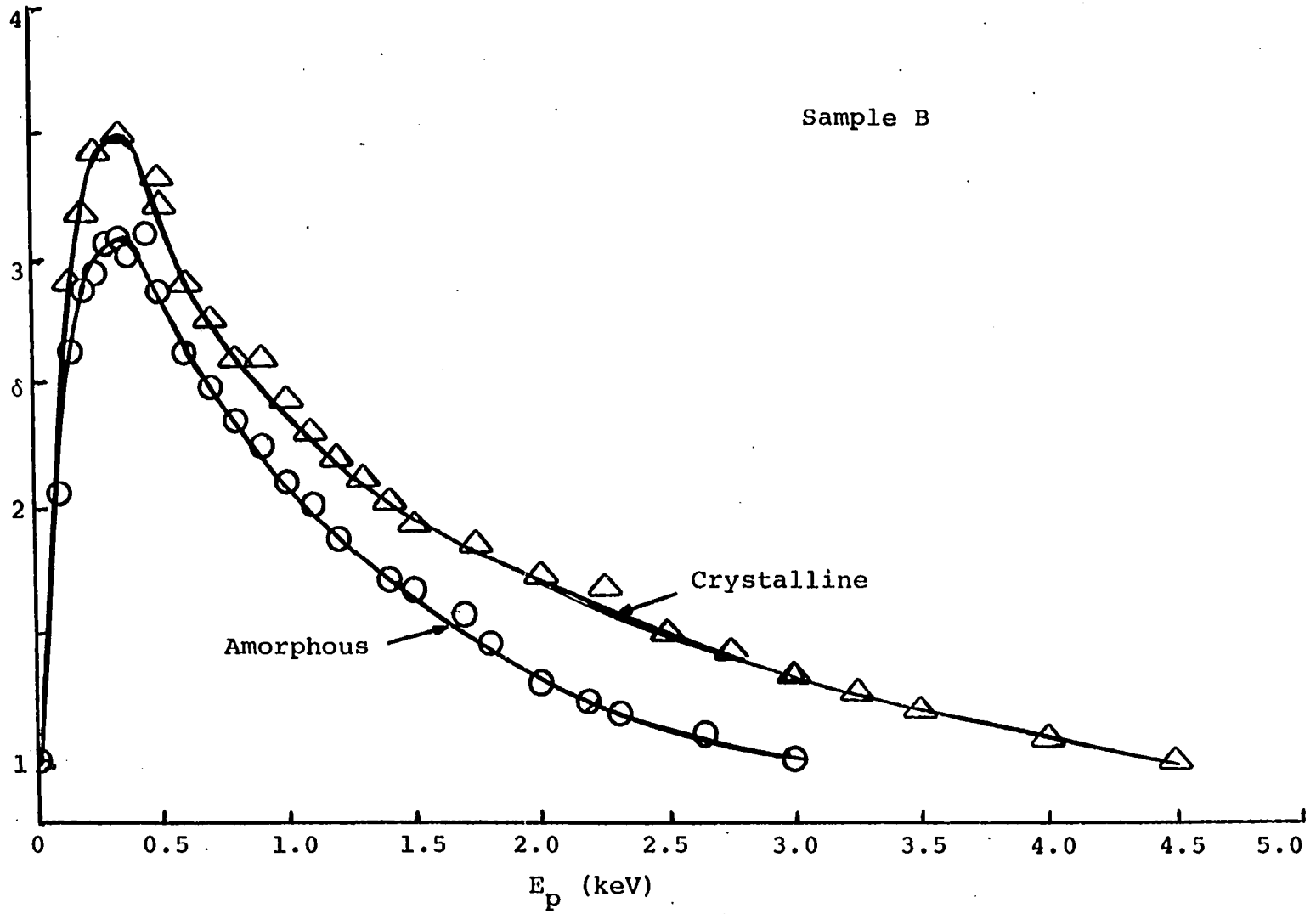

Figure 15. Secondary yield of amorphous and crystalline $Ge_{7.1}As_{61.8}Te_{31.1}$

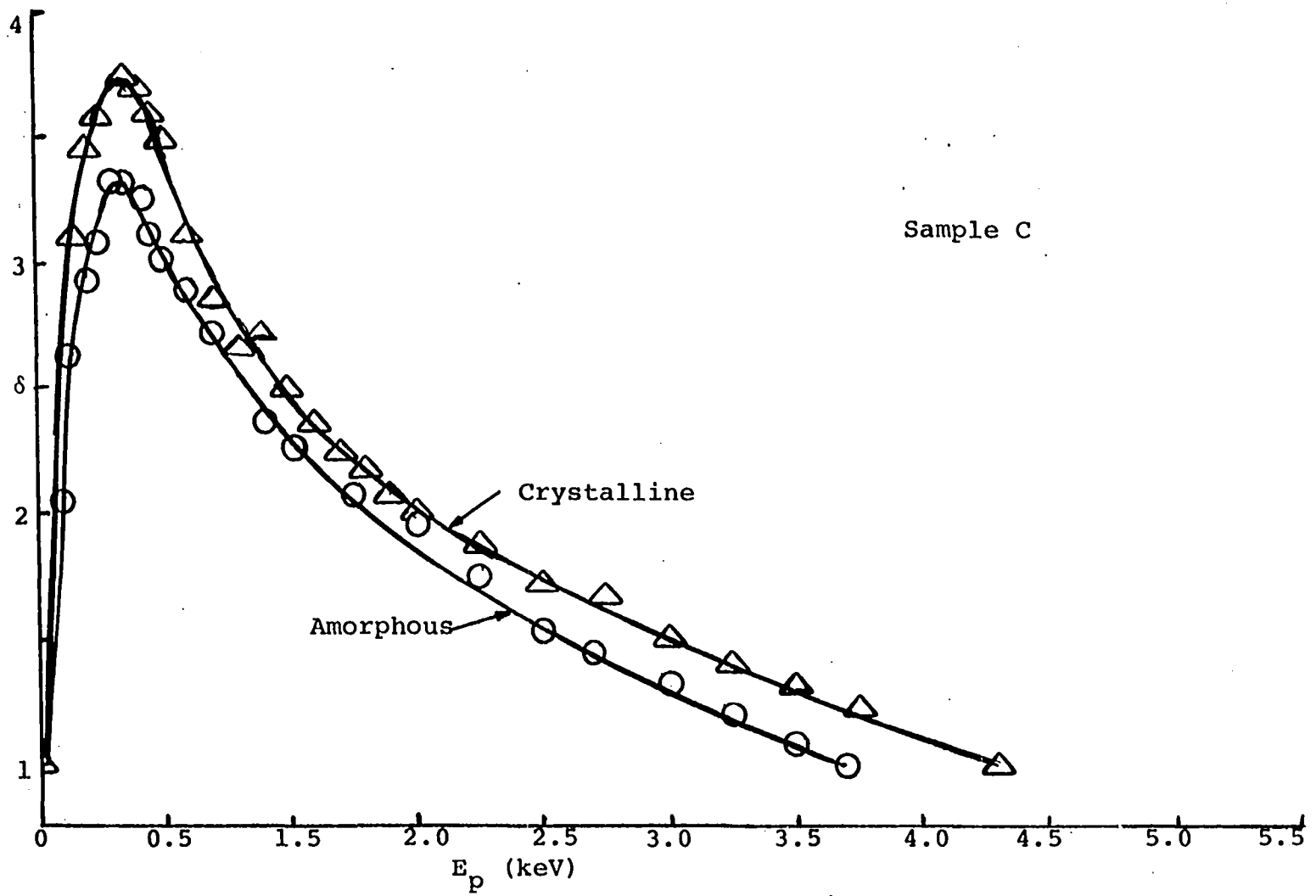

Figure 16. Secondary yield of amorphous and crystalline $Ge_{14.6}As_{27.3}Te_{58.1}$

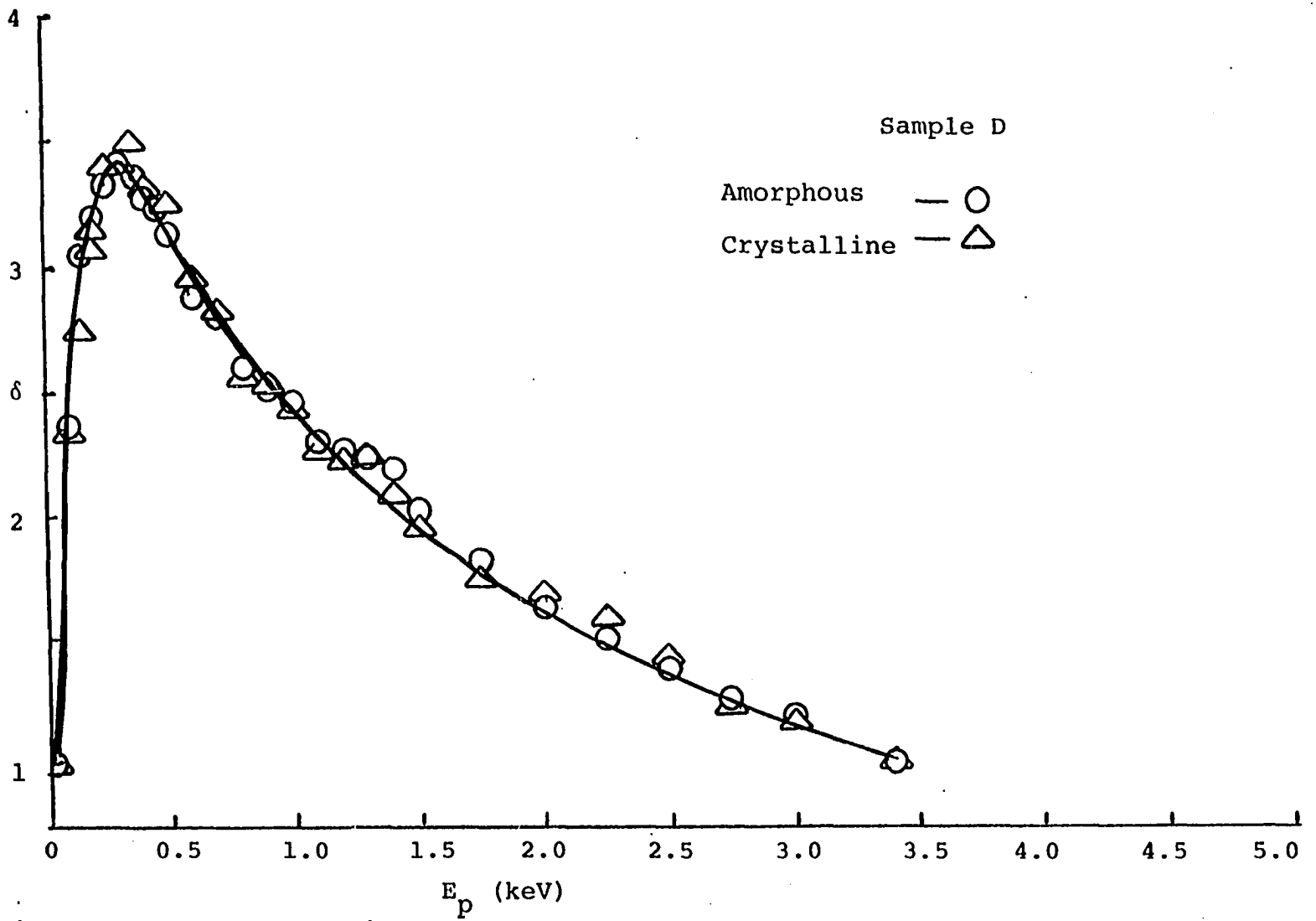

Figure 17. Secondary yield of amorphous and crystalline $Ge_{15.3}As_{21.7}Te_{63}$

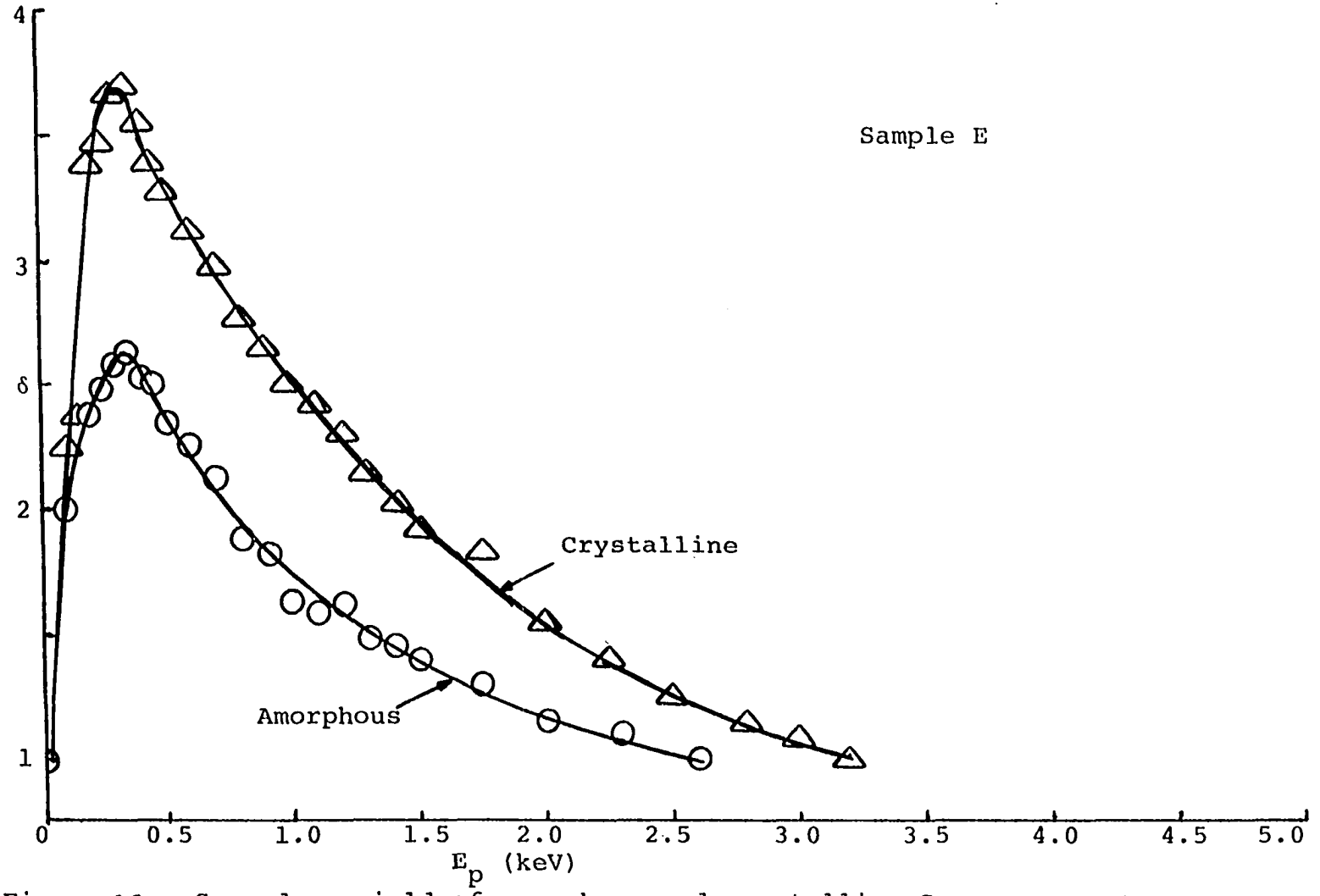

Figure 18. Secondary yield of amorphous and crystalline $Ge_{17.9}As_{40.2}Te_{41.9}$

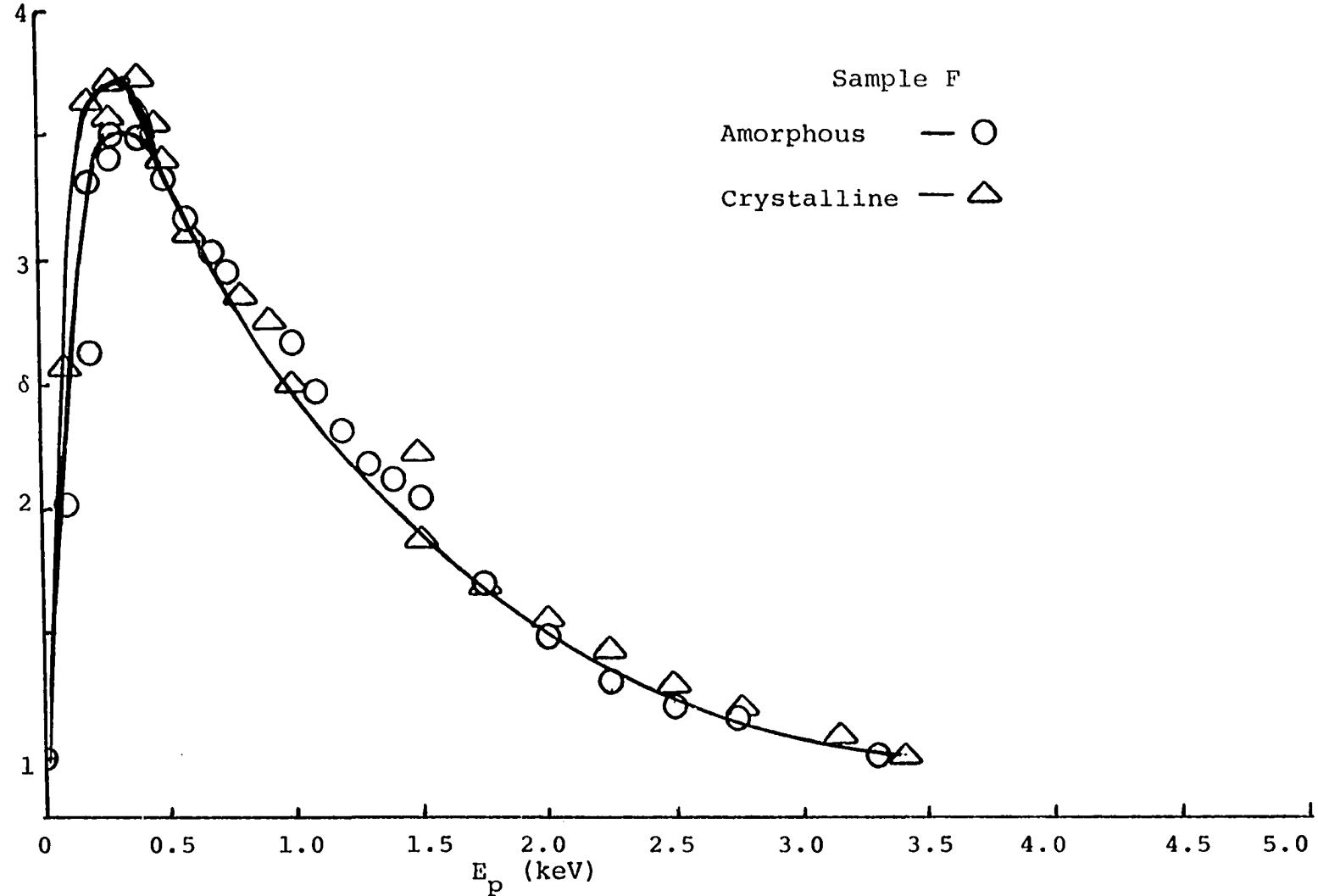

Figure 19. Secondary yield of amorphous and crystalline $Ge_{15.4}As_{37.8}Te_{46.8}$

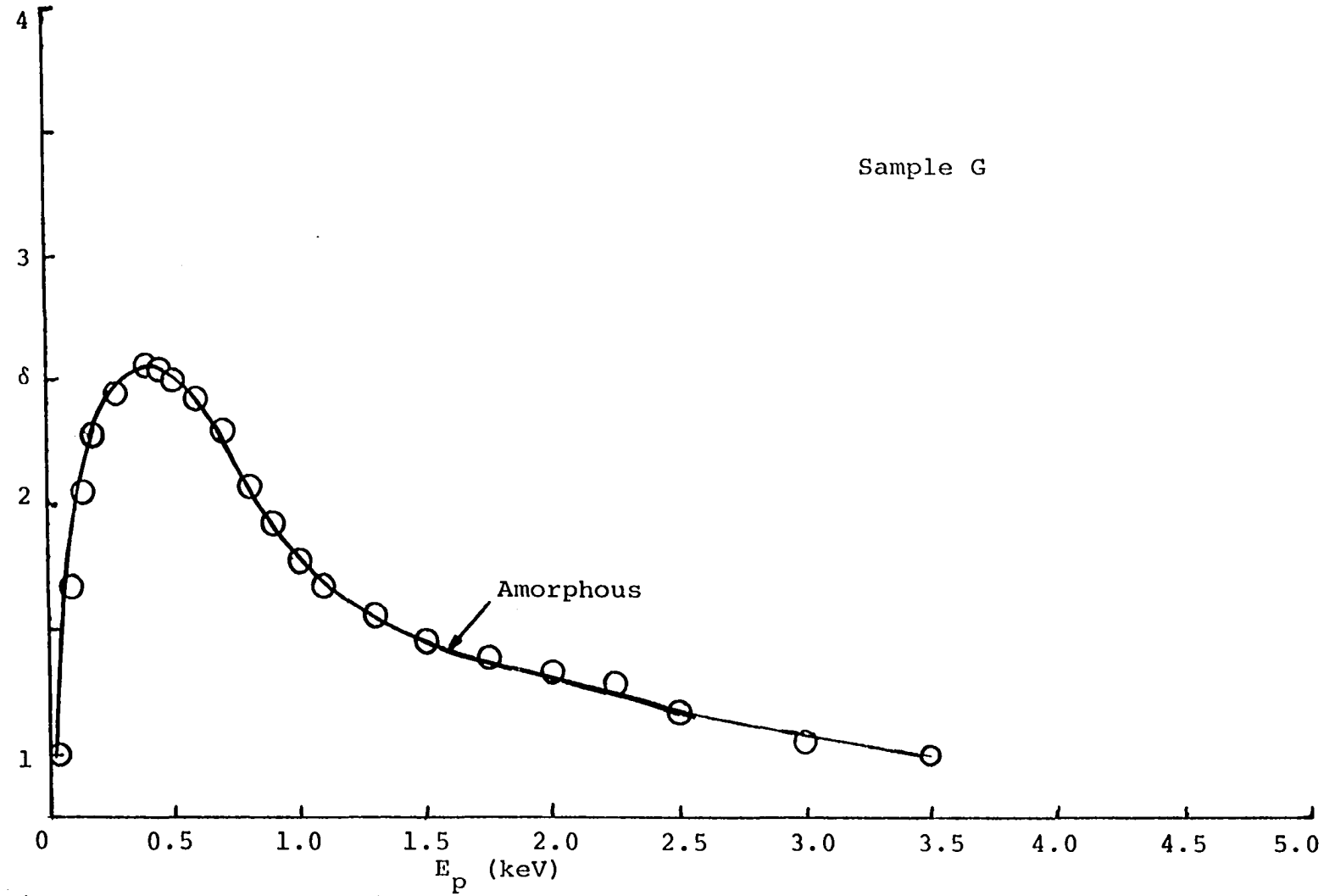

Figure 20. Secondary yield of amorphous $Ge_{0.5}As_{65.1}Te_{34.4}$

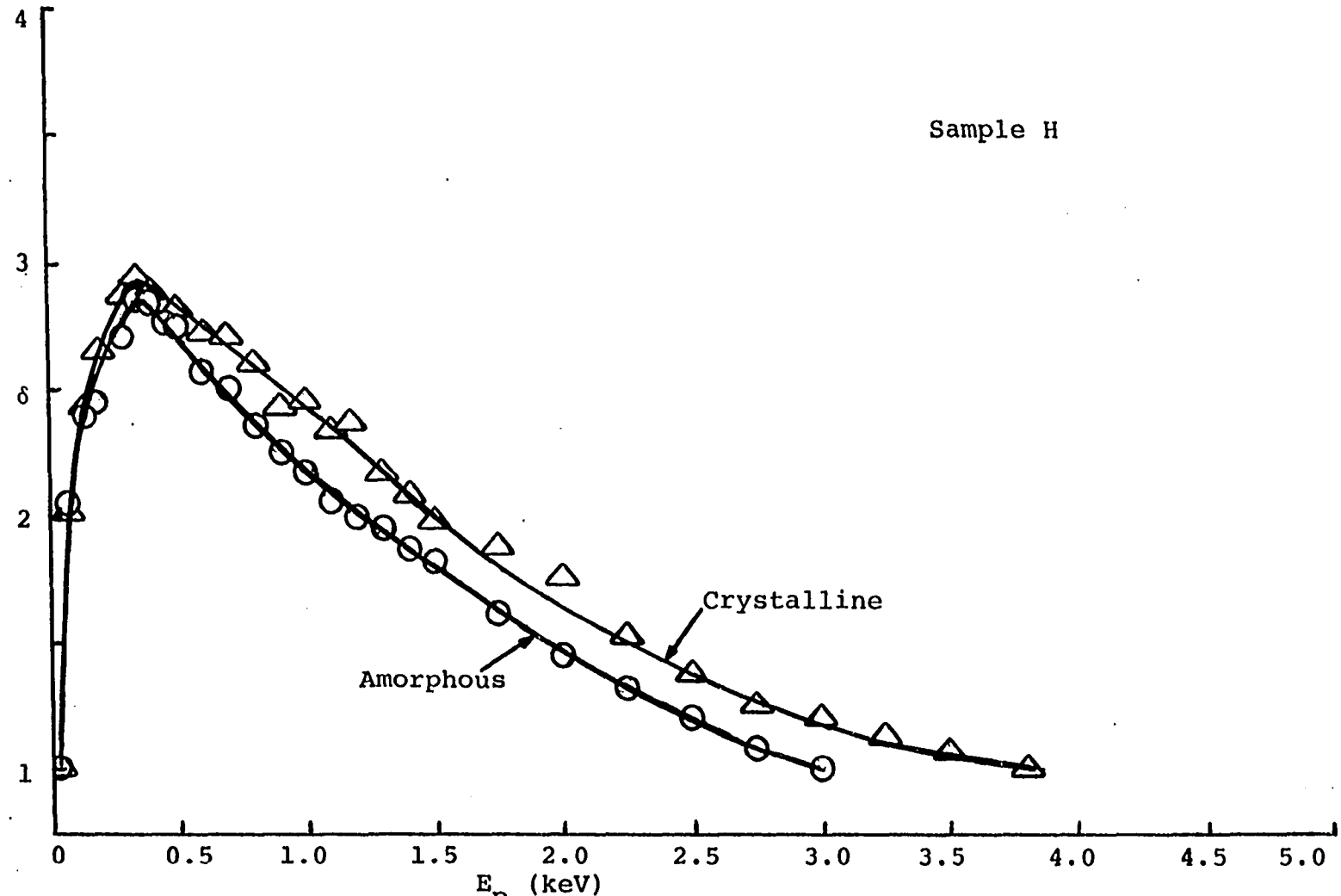

Figure 21. Secondary yield of amorphous and crystalline $Ge_{6.9}As_{67.2}Te_{25.9}$

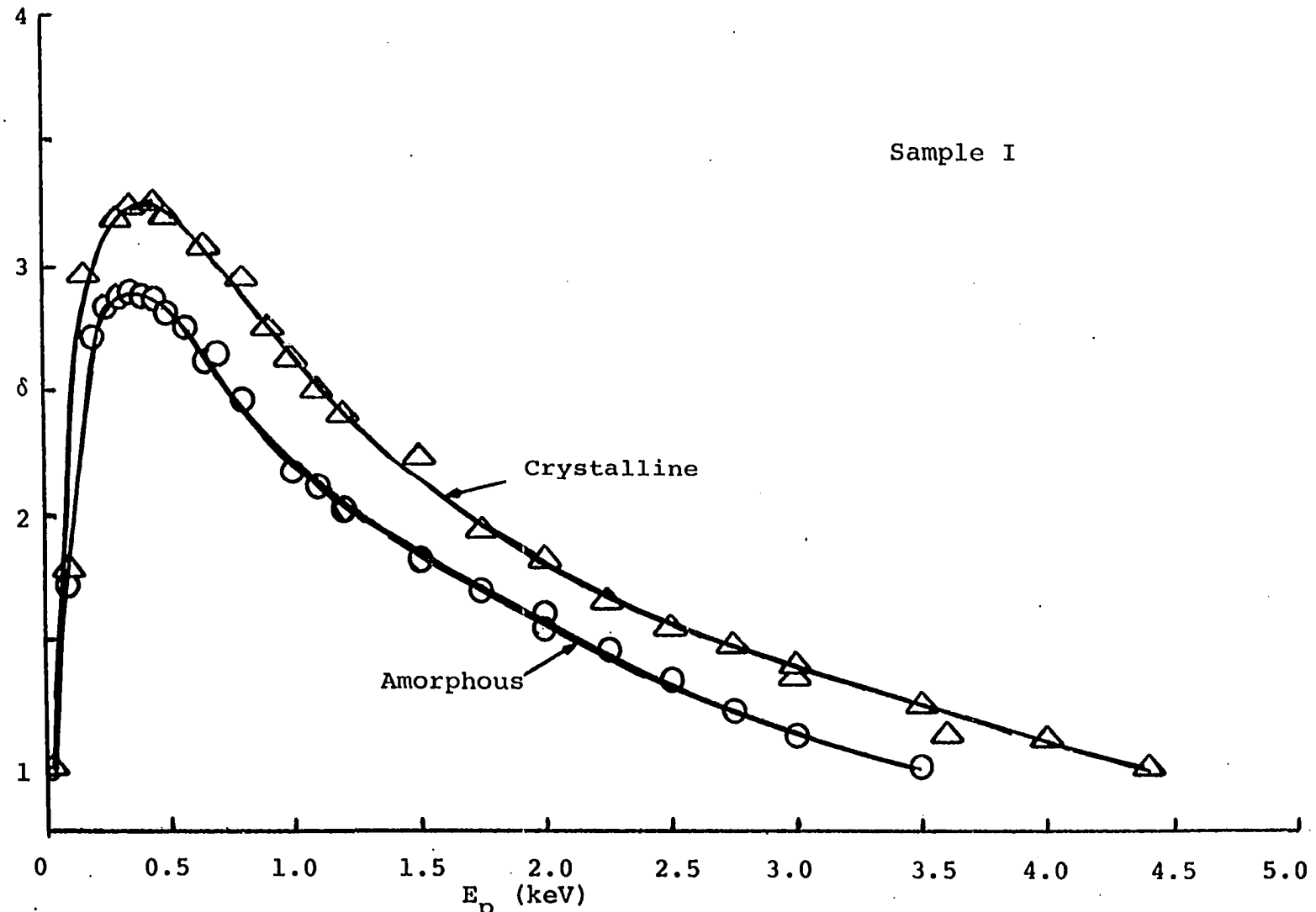

Figure 22. Secondary yield of amorphous and crystalline $Ge_{0.8}As_{36.1}Te_{63.1}$

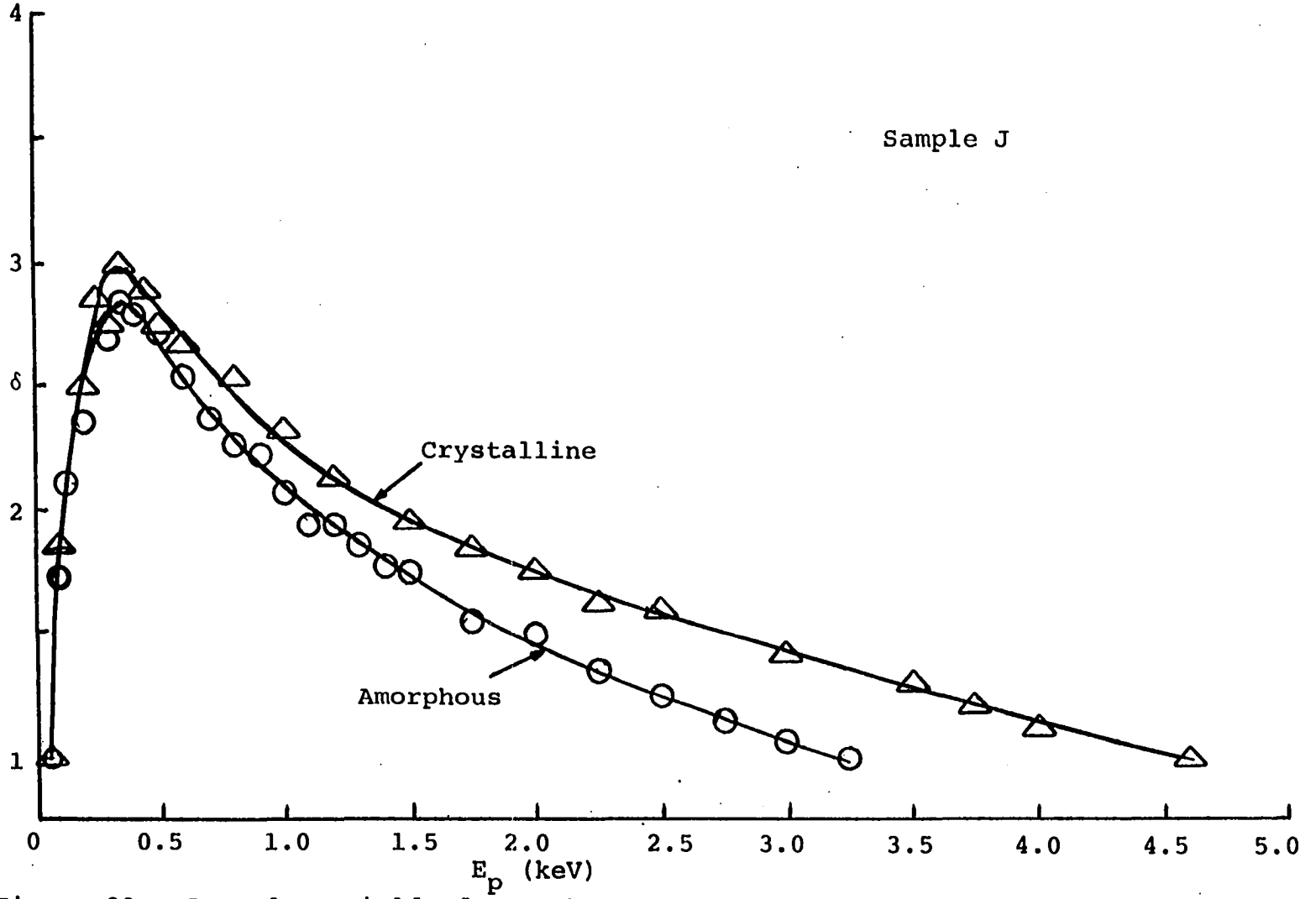

Figure 23. Secondary yield of amorphous and crystalline $Ge_{3.6}As_{42.1}Te_{54.3}$

Figure 24. Microprobe data for crystalline sample C, $Ge_{14.6}As_{27.3}Te_{58.1}$

a. Germanium scanned x-ray output (834x)

b. Arsenic scanned x-ray output (834x)

c. Optical photograph of surface topology (834x)

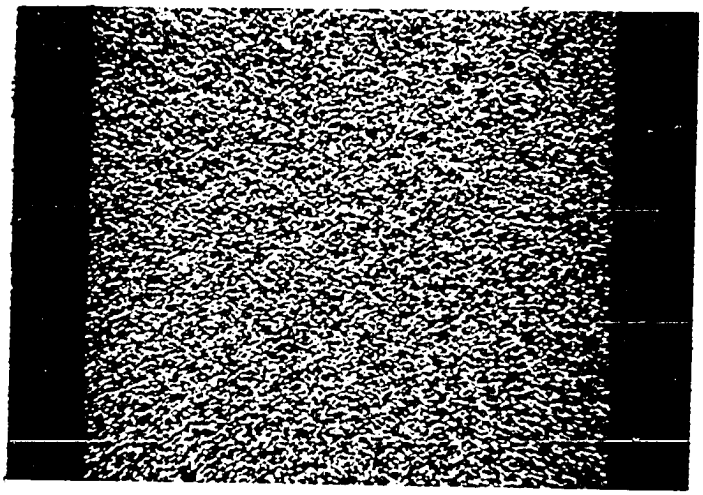

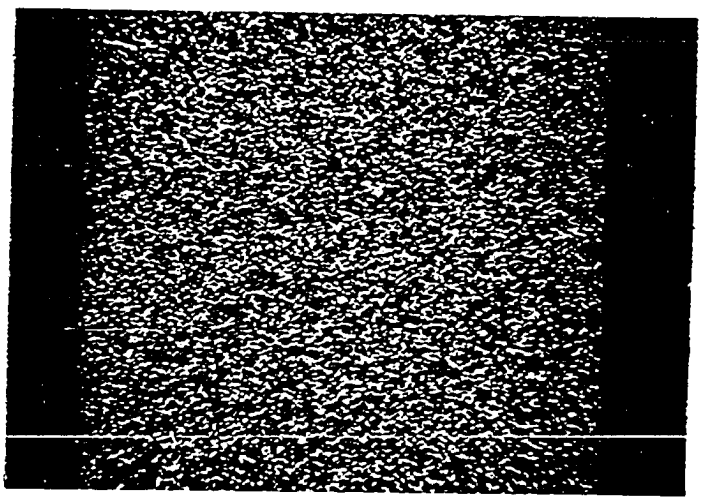

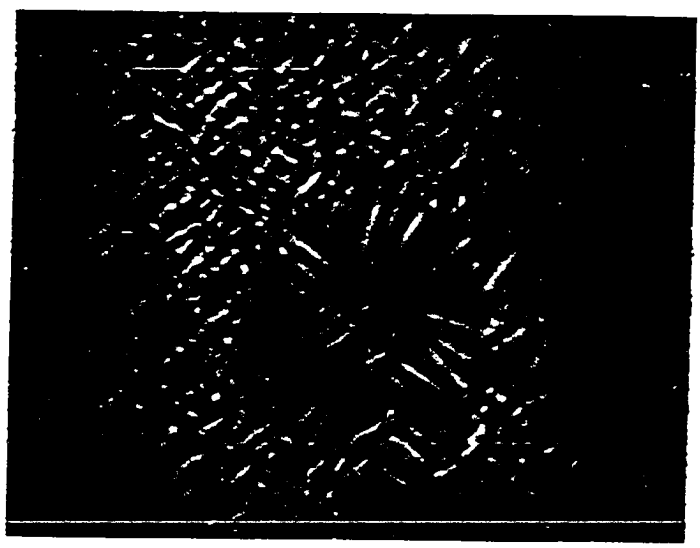

Figure 25. SEM photograph of sample A, amorphous $Ge_{4.1}As_{47.3}Te_{48.6}$ on a glass substrate (1000x at 0° tilt)

Figure 26. SEM photograph of sample A, amorphous $Ge_{4.1}As_{47.3}Te_{48.6}$ on a stainless steel substrate (3000x at 45° tilt)

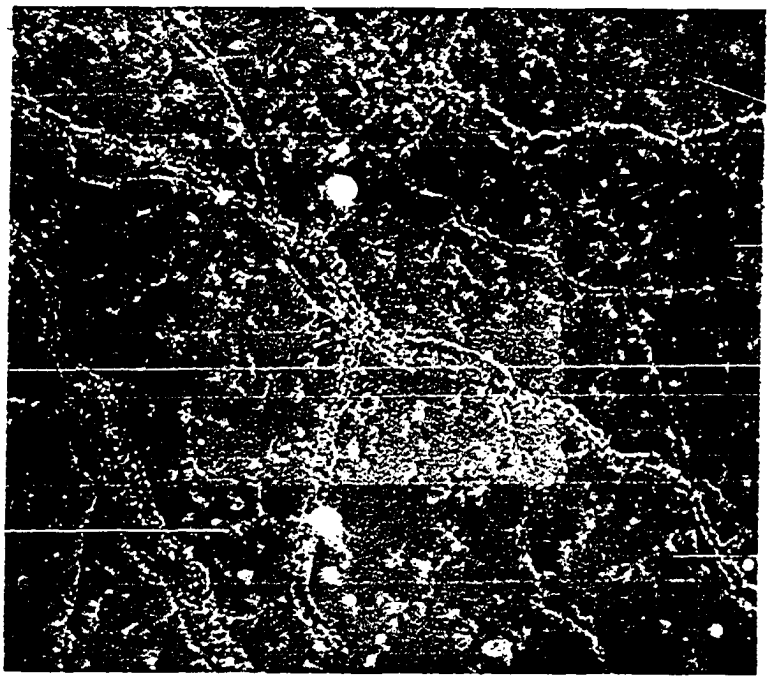

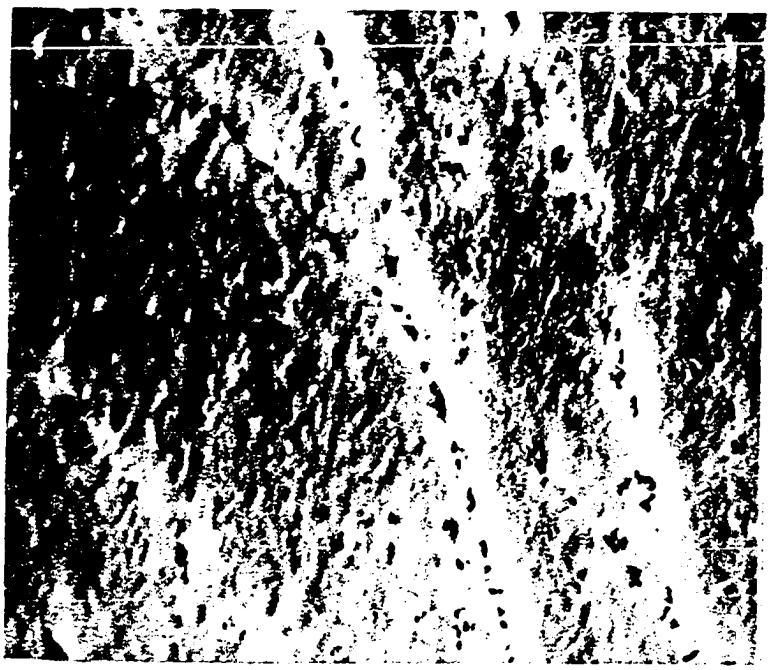

Figure 27. SEM photograph of sample A, crystalline $Ge_{4.1}As_{47.3}Te_{48.6}$ on a glass substrate (1000x at 0° tilt)

Figure 28. SEM photograph of sample A, crystalline $Ge_{4.1}As_{47.3}Te_{48.6}$ on a stainless steel substrate (3000x at 45° tilt)

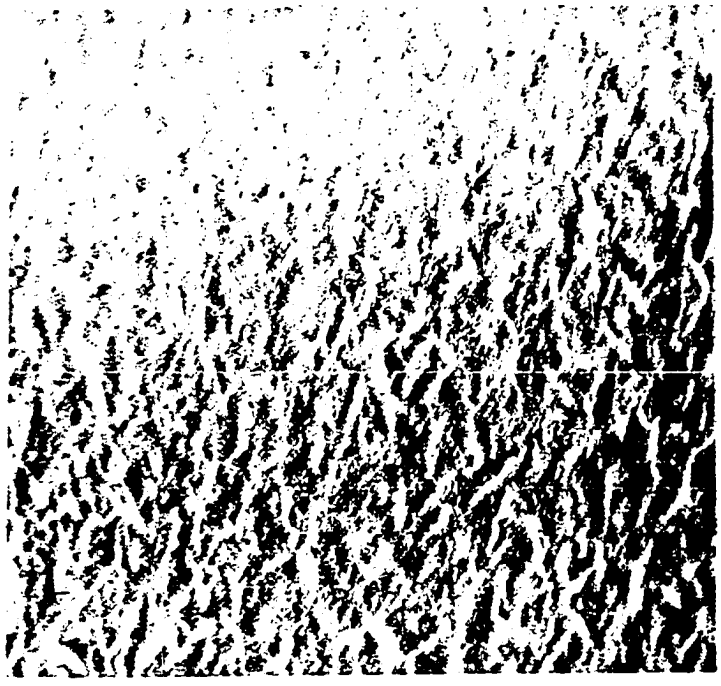

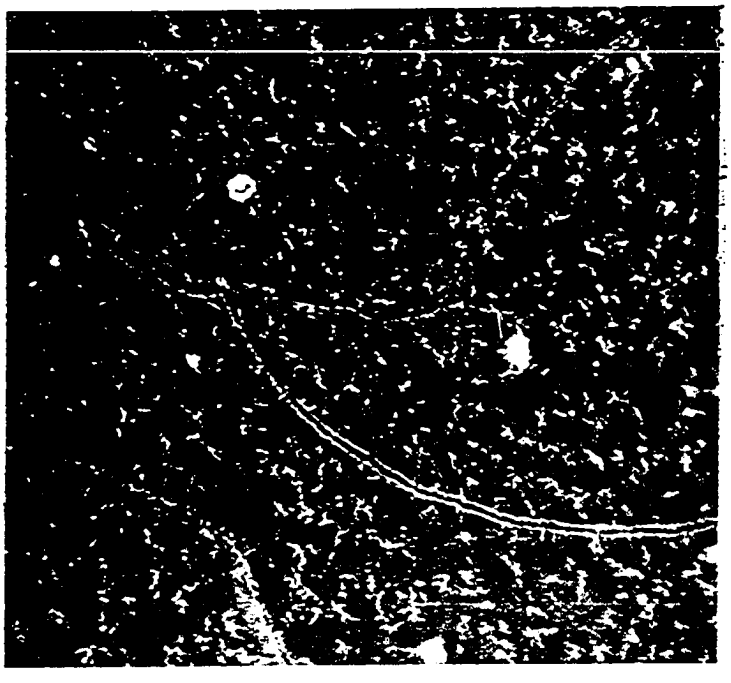

Figure 29. SEM photograph of sample B, amorphous $Ge_{7.1}As_{61.8}Te_{31.1}$ on a stainless steel substrate (3000x at 45° tilt)

Figure 30. SEM photograph of sample B, crystalline $Ge_{7.1}As_{61.8}Te_{31.1}$ on a stainless steel substrate (3000x at 45° tilt)

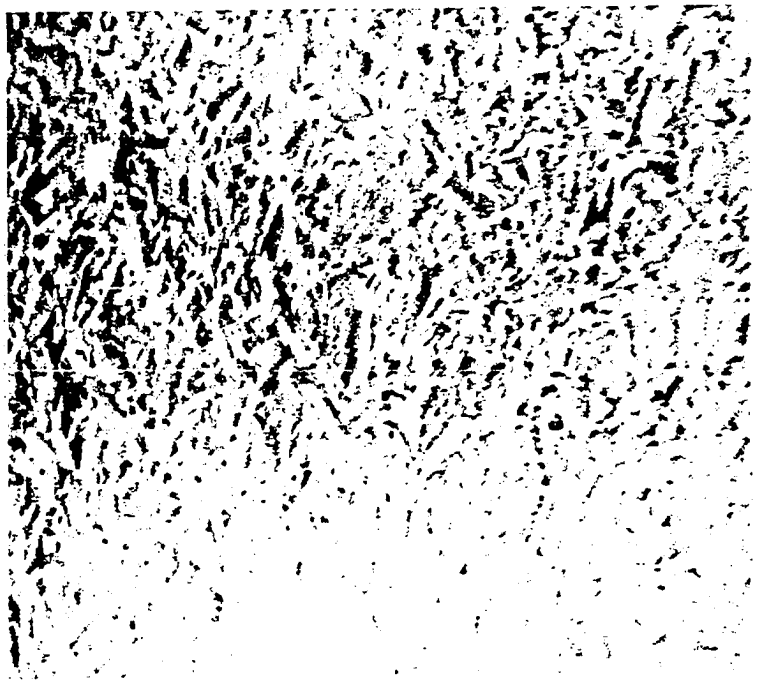

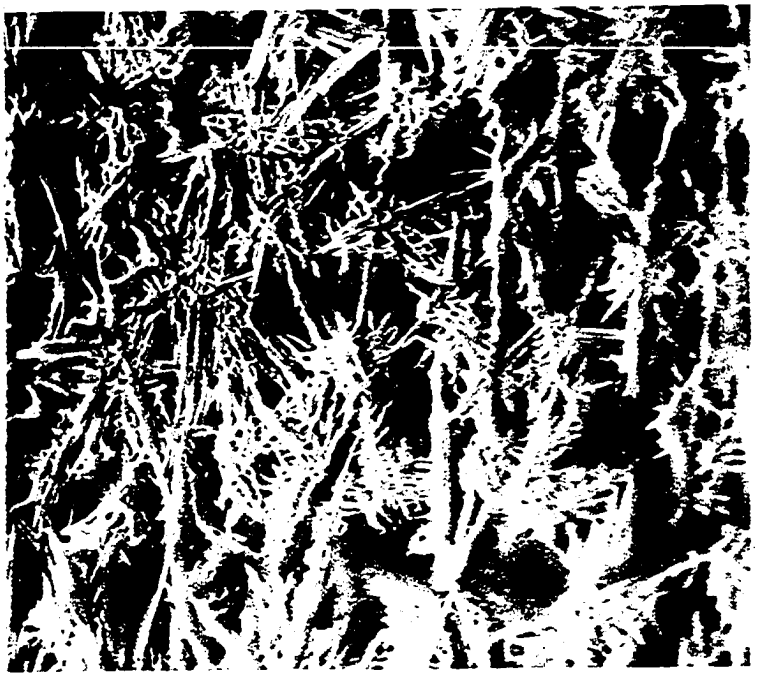

Figure 31. SEM photograph of sample C, amorphous $Ge_{14.6}As_{27.3}Te_{58.1}$ on a glass substrate (1000x at 0° tilt)

Figure 32. SEM photograph of sample C, amorphous $Ge_{14.6}As_{27.3}Te_{58.1}$ on a stainless steel substrate (3000x at 45° tilt)

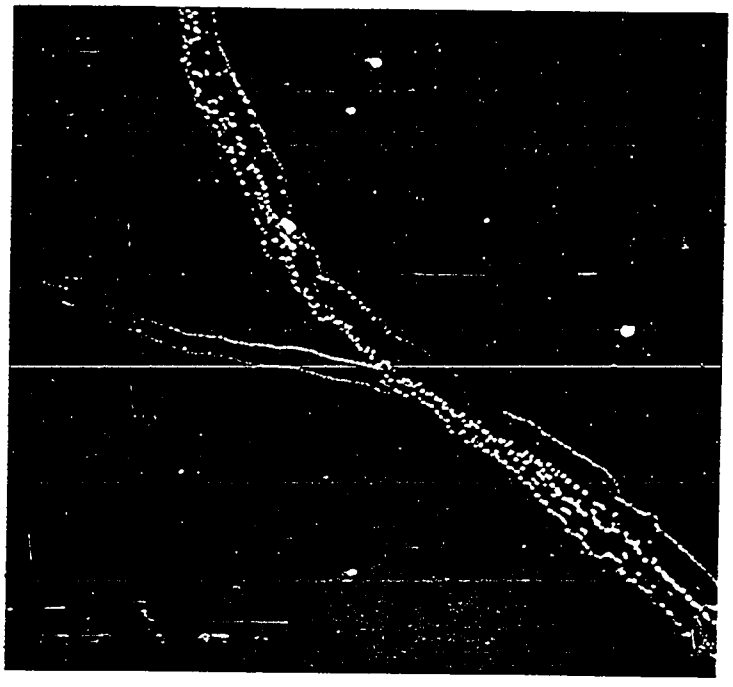

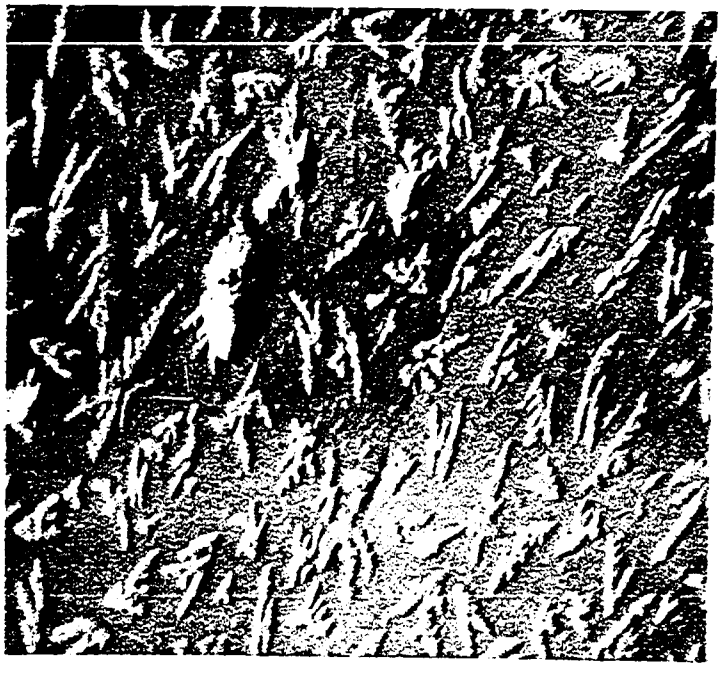

Figure 33. SEM photograph of sample C, crystalline $Ge_{14.6}As_{27.3}Te_{58.1}$ on a glass substrate (1000x at 0° tilt)

Figure 34. SEM photograph of sample C, crystalline $Ge_{14.6}As_{27.3}Te_{58.1}$ on a stainless steel substrate (1000x at 45° tilt)

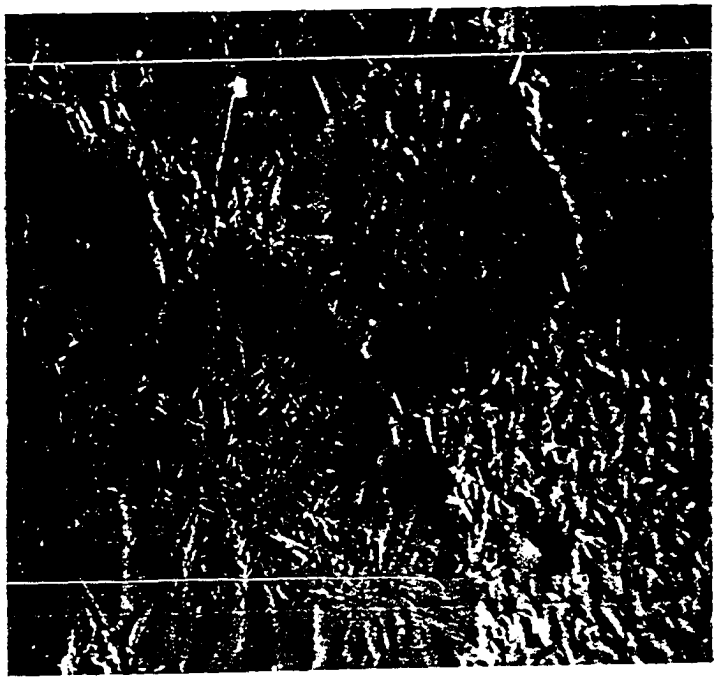

Figure 35. SEM photograph of sample D, crystalline $Ge_{15.3}As_{21.7}Te_{63}$ on a glass substrate (1000x at 45° tilt)

Figure 36. SEM photograph of sample D, crystalline $Ge_{15.3}As_{21.7}Te_{63}$ on a stainless steel substrate (1000x at 45° tilt)

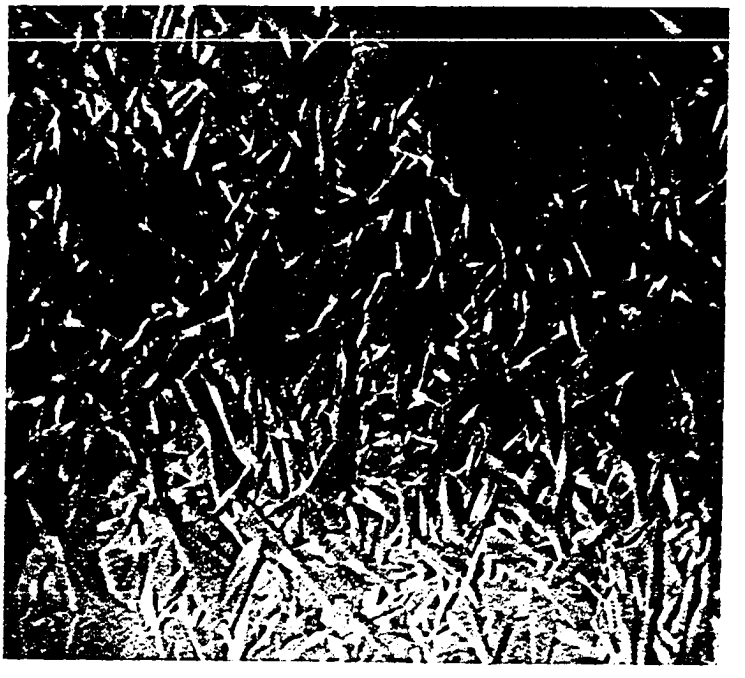

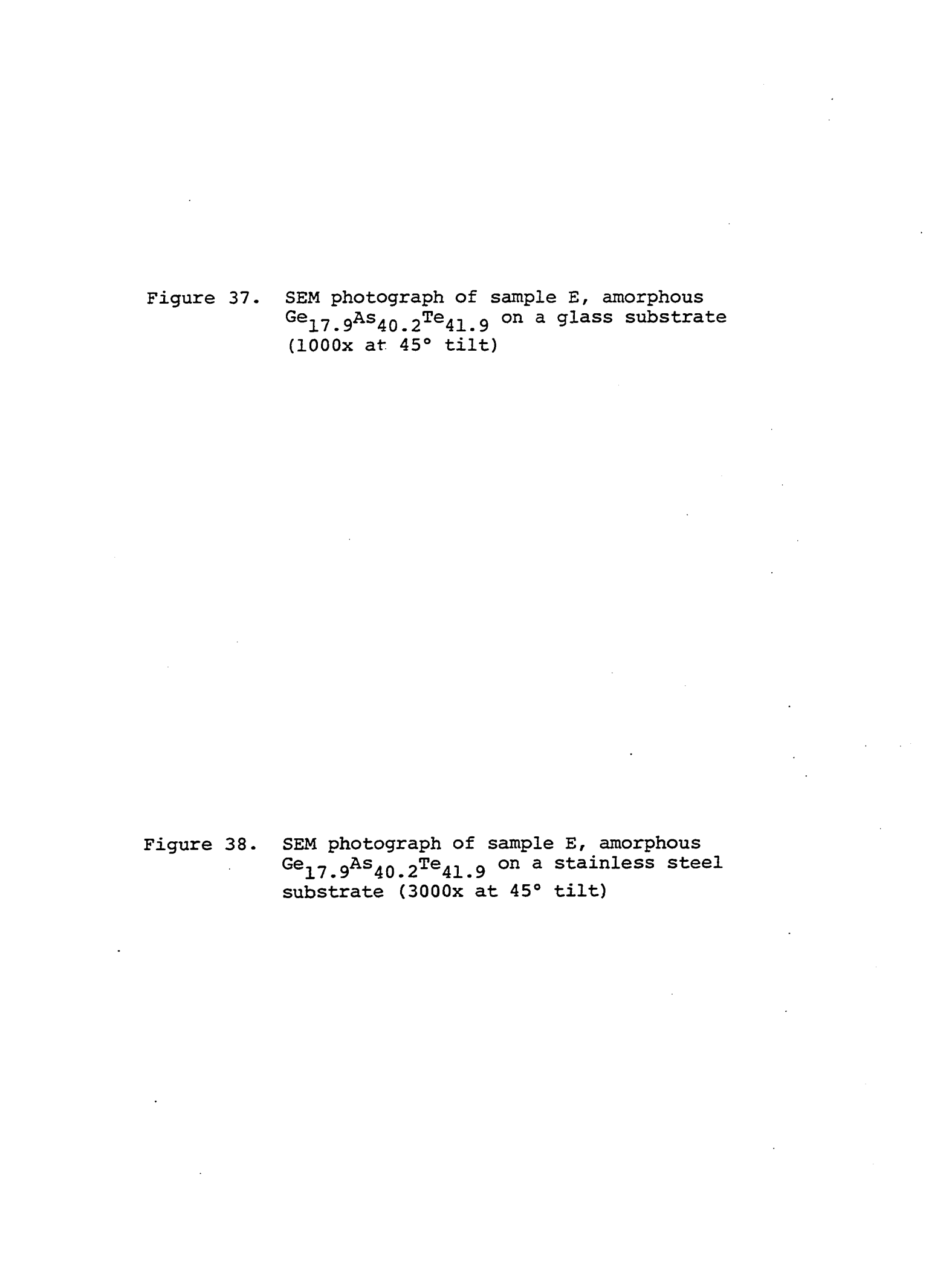

Figure 37. SEM photograph of sample E, amorphous $Ge_{17.9}As_{40.2}Te_{41.9}$ on a glass substrate (1000x at 45° tilt)

Figure 38. SEM photograph of sample E, amorphous $Ge_{17.9}As_{40.2}Te_{41.9}$ on a stainless steel substrate (3000x at 45° tilt)

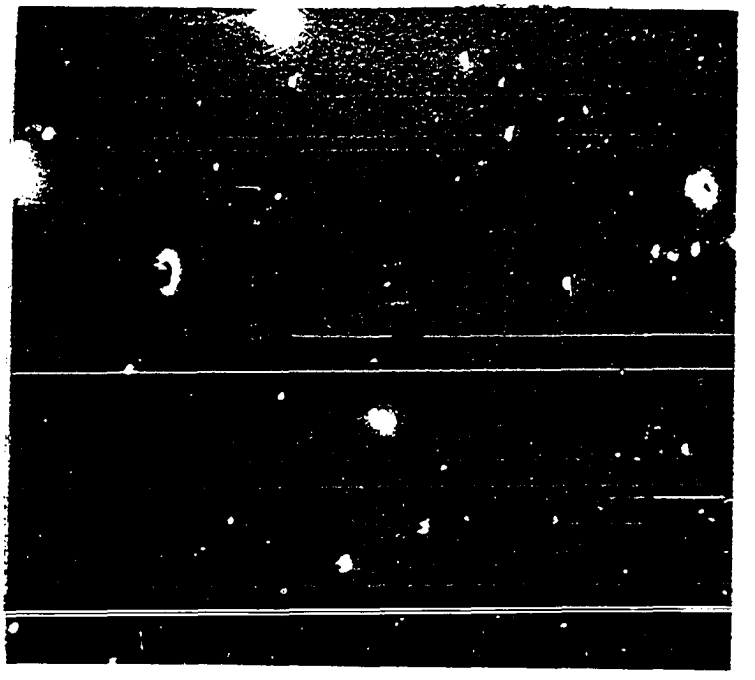

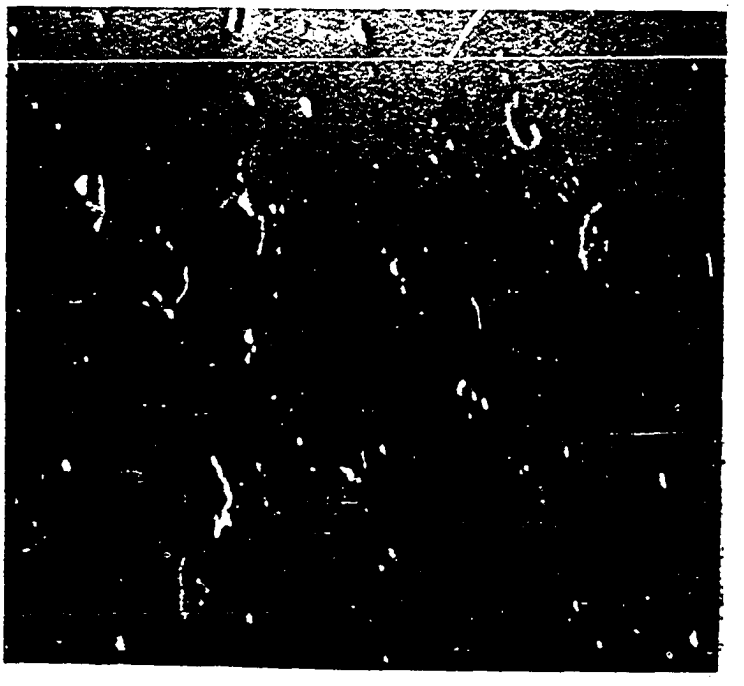

Figure 39. SEM photograph of sample E, crystalline $Ge_{17.9}As_{40.2}Te_{41.9}$ on a glass substrate (1000x at 45° tilt)

Figure 40. SEM photograph of sample E, crystalline $Ge_{17.9}As_{40.2}Te_{41.9}$ on a stainless steel substrate (1000x at 45° tilt)

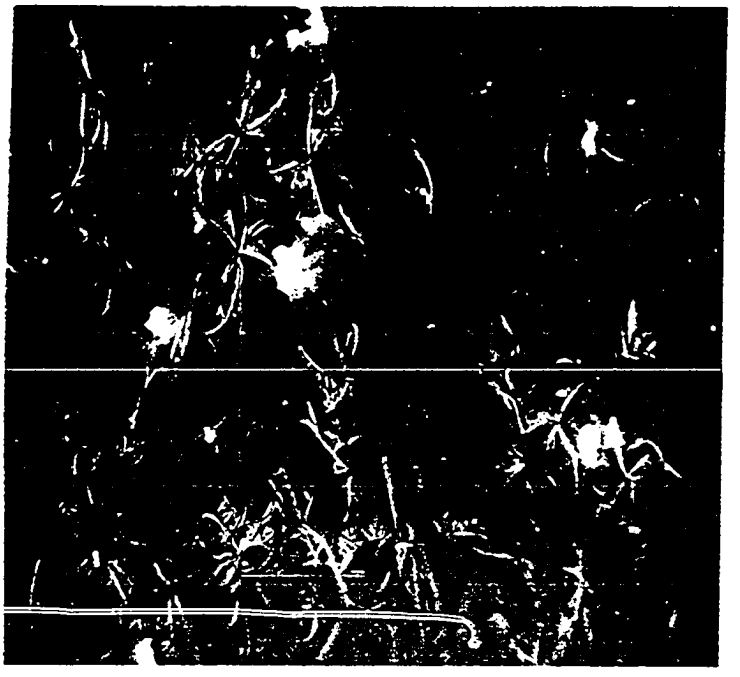

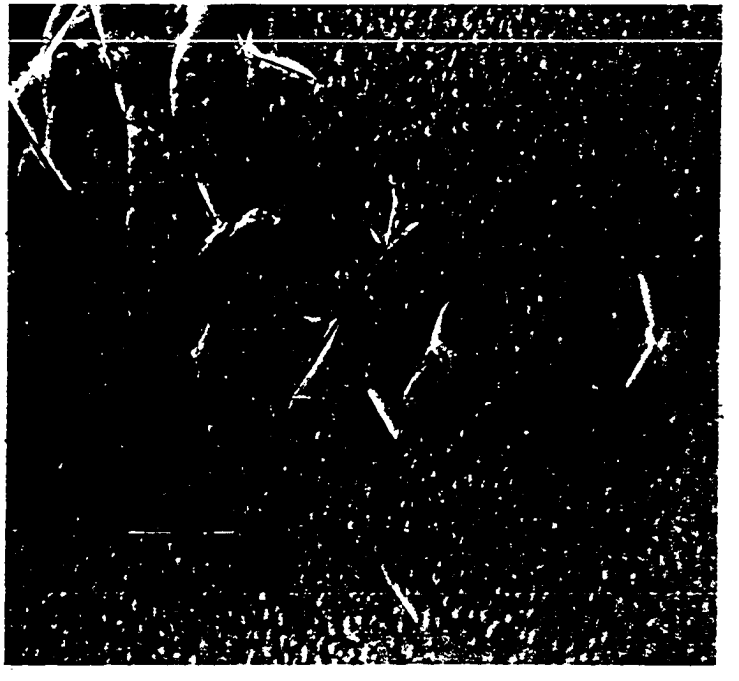

Figure 41. SEM photograph of sample F, crystalline $Ge_{15.4}As_{37.8}Te_{46.8}$ on a glass substrate (1000x at 45° tilt)

Figure 42. SEM photograph of sample F, crystalline $Ge_{15.4}As_{37.8}Te_{46.8}$ on a stainless steel substrate (100x at 45° tilt)

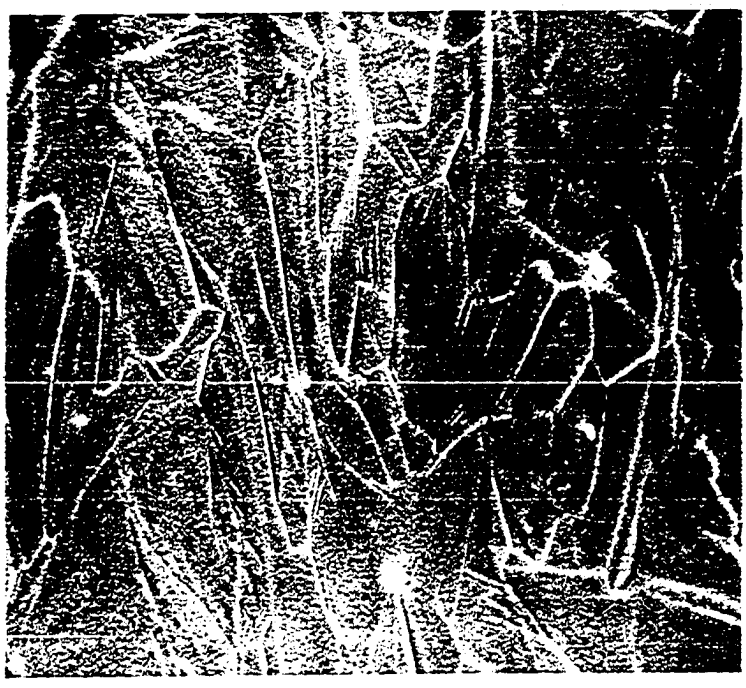

Figure 43. SEM photograph of sample H, crystalline $Ge_{6.9}As_{67.2}Te_{25.9}$ on a stainless steel substrate (3000x at 45° tilt)

Figure 44. SEM photograph of sample I, crystalline $Ge_{0.8}As_{36.1}Te_{63.1}$ on a stainless steel substrate (3000x at 0° tilt)

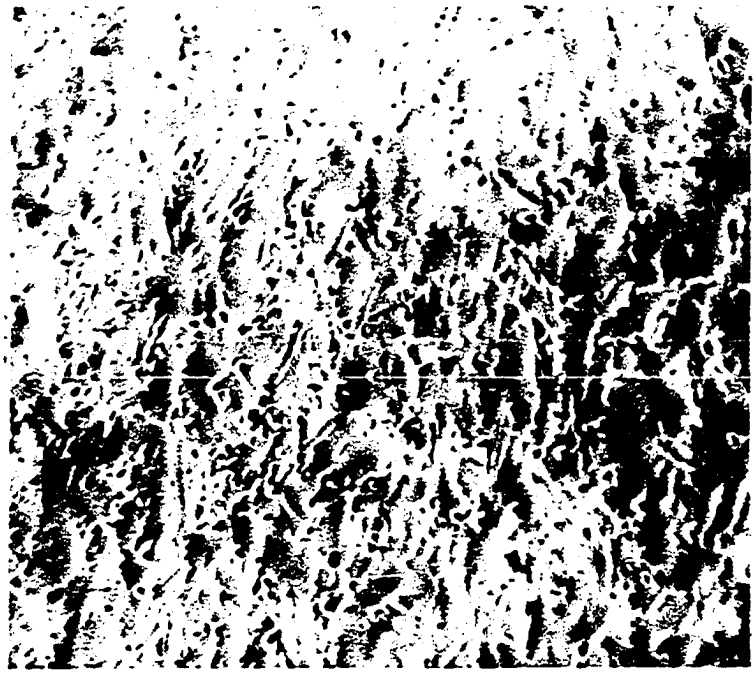

Figure 45. SEM photograph of sample I, amorphous $Ge_{0.8}As_{36.1}Te_{63.1}$ on a glass substrate and sample J, amorphous $Ge_{3.6}As_{42.1}Te_{54.3}$ on a glass substrate (1000x at 45° tilt)

Figure 46. SEM photograph of sample J, crystalline $Ge_{3.6}As_{42.1}Te_{54.3}$ on a stainless steel substrate (3000x at 0° tilt)

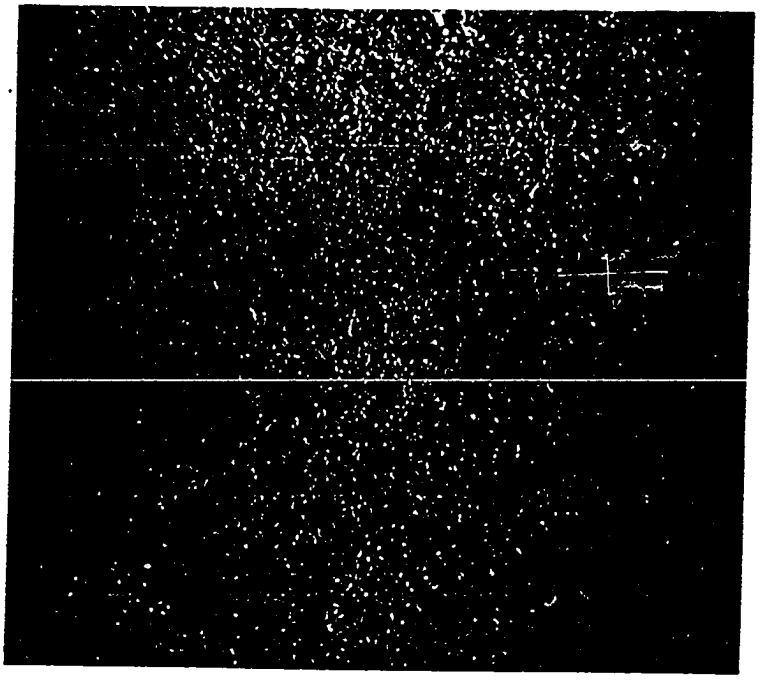

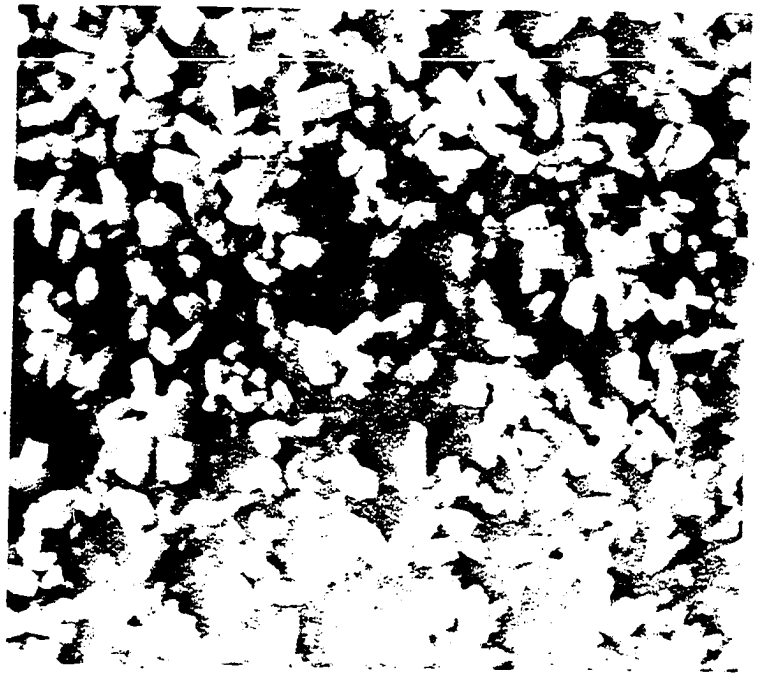

IV. DISCUSSION

A. Application to Memory Systems

One envisioned computer memory (random access high density large capacity) might be fabricated according to the following guide lines. A support plate could be fabricated from a nonreactive nonvolatile metallic conductor as shown in Figure 47. On this surface would be deposited a 1.5 micron layer of a good dielectric. Fused quartz of 100% silicon dioxide has a dc volume resistivity at 25°C of $>10^{19}$ ohm-cm. Holes with a diameter of 4 microns on 6 micron centers would be made in the dielectric to a depth of 1.5 microns. This could be accomplished by using photoresist, masks and either chemical or sputter etching techniques. These holes could also be made by using a high energy electron beam or a laser.

Next, there would be a 1 micron deposition of the threshold type switching material. On top of this would be deposited a thin layer of metal and finally a .5 micron layer of memory material. The metal layer would act as a buffer to slow ion migration between the threshold material and the memory material. Finally, the whole surface would be coated with a thin metal electrode.

This memory would require the stacking of material inside of the memory cell for two reasons. First, the memory material would require at least 2 A current in order to be switched.

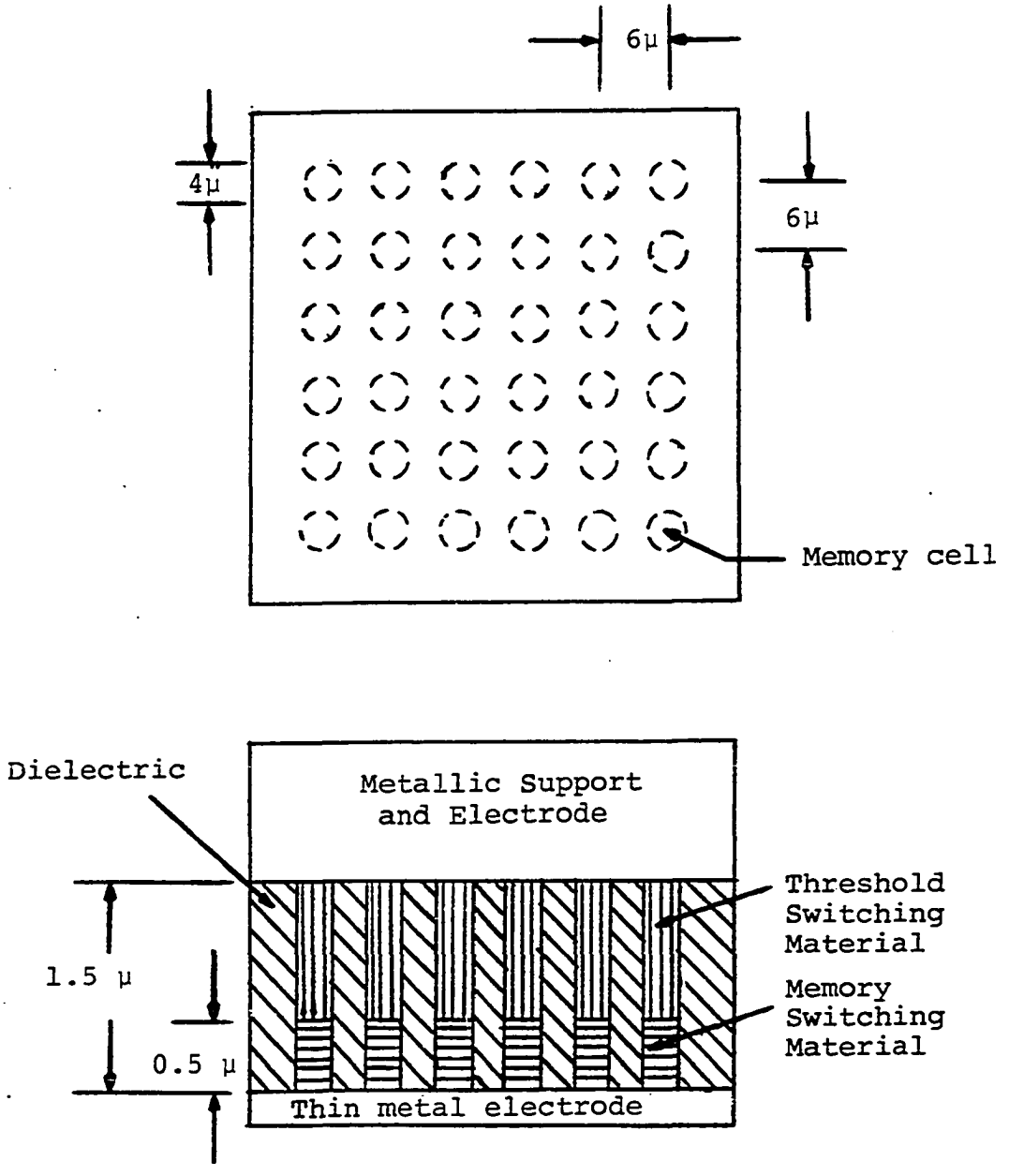

Figure 47. Computer memory layout

Space charge repulsion effects would prevent this current from arriving via an electron beam. Hence, electrodes must be employed in order to deliver this power to the memory cell. But if a cell is already in a conducting state, then it would be a low resistive path between the two electrodes.

For a 1 in. x 1 in. memory structure the number of memory cells would be 1.8×10^7. A memory cell in the amorphous state would have a resistance

$$R_H = \frac{\rho L}{A} = 1.1 \times 10^6\ \Omega\text{-cm}\ \frac{5\times10^{-5}\text{cm}}{3.14(2\times10^{-4})^2\text{cm}^2} = 4.4 \times 10^8 \Omega.$$

While, for the crystalline state it would be

$$R_L = .98\ \Omega\text{-cm}\ \frac{5\times10^{-5}\text{cm}}{3.14(1\times10^{-4})^2\text{cm}^2}$$

$$+\ 1.1\times10^6\ \Omega\text{-cm}\ \frac{5\times10^{-5}\text{cm}}{3.14(2^2-1^2)\times10^{-8}\text{cm}^2}\ .$$

The second term can be neglected because it is much smaller than the first term and the resistance would be $R_L = 156\ \Omega$. The resistivity values are from Uttecht et al. (29).

For the worst possible case with all the cells in the low state and for no threshold material in the cell, the current drain would be approximately 7.5×10^5 A/sq. in. of memory! Hence, the threshold material would be needed. From Hilton et al. (11) the resistivity of $Ge_{10}As_{20}Te_{70}$ is 2.8×10^5 Ω-cm at 300°K. The resistance of this section would be

$$R_T = 2.8\text{x}10^4\ \Omega\text{-cm}\ \frac{10^{-4}\ \text{cm}}{3.14(2\text{x}10^{-4}\text{cm})^2} = 2.23 \times 10^7\ \Omega,$$

while for $Ge_{10}As_{15}Te_{75}$, $\rho = 2\text{x}10^7\ \Omega\text{-cm}$ and

$$R_T' = 2\text{x}10^2\ \Omega\text{-cm}\ \frac{10^{-4}\ \text{cm}}{3.14(2\text{x}10^{-4}\text{cm})^2} = 1.59\text{x}10^{10}\ \Omega.$$

For the worst case the new equivalent resistances would be

$$R_H' = R_H + R_T = 4.62 \times 10^8\ \Omega$$

and

$$R_L' = R_L + R_T = 2.23 \times 10^7\ \Omega.$$

The worst possible case would be when the cell is in state R_L' which gives a current drain of approximately 6.1 A/sq. in. If the leakage through the dielectric is considered then the dielectric resistance would be

$$R_D = \frac{\rho L}{A} = 10^{19}\ \Omega\text{-cm}\ \frac{(1.5\text{x}10^{-4}\ \text{cm})}{(2.54)^2 - \pi(2\text{x}10^{-4})^2 1.8\text{x}10^7\text{cm}^2}$$

$$= 3.57\text{x}10^{14}\ \Omega.$$

This would produce a current of only $2.1\text{x}10^{-14}$ amps and could be neglected.

The current computations were based upon the fact that the electric field must be at least $5\text{x}10^5$ V/cm from Kao (12) in order for switching to occur. For the 1.5 micron thickness the voltage required is 7.5 volts. The power supply requirement is thus established and is quite practical.

The electron beam would be used to switch the cell from the R_L' state to the R_H' state by heating and without the presence of the critical field. The electron beam would require approximately 25 keV in order to penetrate the whole memory cell. This is based upon using the empirical relationship for the penetration depth (R) from Kaplan (13)

$$R = 412\ T_0^{1.265-0.0954\ \ln T_0}$$

where R is in mg/cm^2 and T_0 is the electron energy in meV. This equation is valid for aluminum and dictates that the penetration depth of a 25 keV electron is approximately 4 microns. Since the glasses are of greater density then Al, this incident energy would be adequate to penetrate the 1.5 micron depth of the memory cell.

The energy input needed to heat the cell to above the glass transition temperature needs to be found. The volume of a memory cell would be 1.88×10^{-11} cm^3. The specific heat per unit volume is 4.5 $\frac{joules}{cm^3\ °K}$ from Hilton et al. (11) and Warren (30). The energy input needed would be 8.45×10^{-11} joules/°K. The total energy required would be dependent upon the mechanism of filament growth since the filament growth places a restriction upon the ambient temperature.

Warren and Male (31) have shown that as the temperature is increased the critical field required for switching decreases. For the 4 micron diameter memory cell the relative

critical field curve that corresponds to this will be midway between two of their curves. The electric field difference for the memory cell between 350°K and 220°K is a factor of 5. Hence, filament growth can occur in the memory cell if the field supplied by the electrodes is less than the critical field and if upon heating up of the cell by an electron beam the applied field exceeds the critical field.

After the filament has been grown, the applied field would be turned off and the threshold material would return to the amorphous state. Upon reapplying the field, no switching would occur because the temperature would have returned to ambient and the field would still be less than the critical field of the threshold material, even though, most of the voltage drop would be across the threshold material.

If the material needed to be heated to 350°C then the energy input requirement would be [8.45×10^{-11} joules/°K] × (330°K) = 2.79×10^{-8} joules. To get some feel for the kind of electron beam and the time required to produce this amount of heating, assume that 25 keV electrons at 10^{-8} amperes are to be used. The energy in a 25 keV electron is 4×10^{-15} joules. Assume that 10% (this is a very pessimistic value and 50% is more realistic) of the electrons energy is utilized for heating then it would be found that 6.95×10^{7} electrons would be needed to accomplish this heating. A beam current of 10^{-8} A would require about 110×10^{-6} seconds to deliver this number

of electrons. This time could be decreased by preheating the substrate so that the ambient temperature is 250°C. This would be reflected as a 36×10^{-6} second switching time.

There would be no trouble with the state determination by secondary electron emission, as long as, the top electrode remained thin. A thick electrode would obscure the secondary electron information by blocking their transmission to the secondary electron monitor. If an electron beam of 1 keV is used, then the electron velocity would be 1.88×10^{7} m/sec. The transit time for an electron of this energy would be 1.62×10^{-8} sec/feet. This would not govern the rate at which this memory could be interrogated but the transit time of the secondary electrons would, because they are of very low energy. The velocity of a 5 eV electron is 2.27×10^{-7} sec/feet. It would be imperative to locate the secondary electron monitor as close as possible to the memory. In fact, this memory could be surrounded by one continuous or several secondary electron monitors. This would minimize the distance traversed and would provide a larger output signal.

Otherwise, the transmitted electrons would be analyzed and many of these problems eliminated. The transit time for secondaries would be eliminated as an example. There would have to be some analysis done on the effect of stacking two memory materials on the transmitted electron current.

If the memory were to be used only for archival storage

applications, then the fabrication would be drastically changed. Chen and Wang (5) have discussed this application in some detail and presented some data on the limitations of this system. The work is a result of a computer program study of the heating dynamics in chalcogenide glasses and the limitations of electron beam optics. The reasons that this application is so appealing is that this memory would have high density, electronic access speed, NDRO, non-volatility, permanency, and radiation resistance. This memory also would have the advantage that no cell demarcation during fabrication would be needed. Hence, construction costs would be greatly reduced. The material would be switched by utilizing the thermodynamic characteristics of the glasses. Again, readout would be accomplished via secondary electron emission.

B. Results and Experimental Methods

The glass deposition techniques affect the composition of the samples as shown by Robertson and Owen (22). For the As_2Te_3+Si system with the atomic percent of silicon being 40, the bulk resistivity was 10^8 Ω-m, the resistivity of a sample prepared by the powder flash evaporation from a hot Mo filament was 10^6 Ω-m, the resistivity of a sample by the electron beam evaporation from a melt was $2x10^5$ Ω-m, and the resistivity of a sample prepared by the glass enclosed in a resistance-

heated Mo boat was $2x10^4$ Ω-m. Sample preparation is extremely important and the difference in the vapor pressures of the elements during deposition, obviously, leads to composition variation. In order to avoid this problem, a sputtering technique should be employed. In fact, a sputtering method would be the best way to make large uniform samples. The resistivities reported in Table 2 for the samples investigated are in agreement with Hilton et al. (11).

The two electron gun technique employed in making these measurements can be criticized because it does conduct the measurements in a forced steady state manner. The surface of the target for measuring semiconductors is clamped at a negative potential. This causes a current to flow through the material. This current and the electric field due to the surface potential may drastically affect the secondary electron emission processes. The secondary electrons have to escape through the surface barrier. The increased barrier due to the flood gun may prevent some of the low energy secondary electrons from escaping. This effect will be minimized if the surface potential due to the flood gun is kept small. Of course, the pulsing techniques have their problems because the incident electrons have a varying potential and the escaping secondaries also see a varying surface potential. The first crossover for all of these glasses is in the range of 20 V to 40 V. This is in agreement with the results presented by Ooka, Dunn, and

Mackenzie (20). Hence, the surface potential has to be less than this and was, in fact, kept at -10 volts.

The secondary yield did not change in all cases as shown in Table 3. The δ_{max} for the crystalline state was always equal to or greater than that for the amorphous state. This is in agreement with Makedonskii and Pustovoit (17) but disagrees with Chen et al. (5). In order to resolve this discrepancy, the process of secondary electron emission must be investigated.

Dekker (6) has developed an elementary theory of secondary electron emission that explains its basic features. The process can be broken down into two parts: the generation of secondaries and their subsequent escape. The production of secondaries is a function of the primary electron characteristics (energy, angle of incidence) and the type of material (composition, ordering and band-gap). The escape probability is a function of the secondaries and the properties of the media. For metals the theoretical description stands on firm ground. However, for insulators the theoretical treatment is inadequate because secondary production involves the excitation of electrons in the filled band and an accurate representation of the wave function for these valence band electrons has not yet been developed. If the wave functions for highly ordered dielectrics have not been developed, then the wave description of amorphous and polycrystalline materials obviously has not

either. Qualitatively, however, the nature of secondary emission for both metals and insulators may be explained rather well.

Metals, generally, have low yield values between 1.0 and 1.5 for δ_{max}. Their yields should be high because of fairly large atoms, loosely bound outer electrons and relatively low ionization potentials. The generation of "free" electrons requires very little energy because the valence and conduction bands overlap. The low δ must then be a result of low escape probability. Due to band overlap, secondaries are able to interact with free electrons which results in a relatively high average energy loss suffered by the secondaries. Thus, metals are characterized by small escape depths.

Insulators, commonly, are compounds which have typically very high bond strengths and ionization potentials. Electrons are much more tightly bound in an insulator than in a metal, hence, the generation of secondaries is lower. Free electrons are hard to create because of the band gap.

The fact that insulators have a higher yield than metals must be on account of a higher escape probability. In insulators secondaries do not interact with lattice electrons (a high energy loss mechanism) because the band gap energy is greater than the average energy of a secondary. Therefore, the primary energy loss mechanism is with phonons or lattice vibrations (a low energy loss mechanism). Thus, insulators with low surface barriers are characterized by large escape

depths.

The amorphous state can be visualized as having a continuous distribution of states through the forbidden band between the conduction band and the valence band. Hence, the properties will be somewhat of a compromise between those of the metal and the insulator because of relatively large atoms, some loosely bound electrons and a competition between high and low energy loss mechanisms. Also, surface barrier energy (electron affinity) and surface roughness must be considered. Therefore, the yield will be dependent upon which of the above mechanisms dominate.

The polycrystalline state will have a surface that is formed via the union of crystallites. The implication of this is that the surface will be, in general, rougher than the amorphous state. The scanning electron microscope pictures of the samples studied verify this. Surface roughness is discussed by Bruining (3) and Ooka et al. (20) and as the surface gets rougher the yield decreases.

Consequently, a priori knowledge of secondary yields of amorphous and polycrystalline material is not known. Use of a random interaction probability with a density of states distribution that is uniform across the band gap might yield some insight. At present the results are not predictable based on any qualitative analysis so far developed, except that the results of this work show that the yield of the crystalline

state is equal to or greater than the amorphous state.

The results of Tables 2 and 3 were cross correlated for any trends. No interrelationships appeared and upon plotting this data (δ_{max} versus E_{pmax}) the points were comparable but slightly higher than those reported by other investigators for glasses. Barut (1) has compiled this data and the range is from 2 to 3.5 for δ_{max} and from 300 to 450 volts for E_{pmax}. The samples investigated in this work ranged from 2.57 to 4.95 for δ_{max} and from 300 to 450 volts for E_{pmax}.

The microprobe results verified the uniform distribution of the elements in the samples. This is to be contrasted with the results for the bulk samples that lie near the border of the glassy region. Sample E was prepared with the formula $As_{50}Te_{30}Ge_{20}$. This material lies on the border to the glassy region. The sample was cooled in air and a chunk of it was analyzed by microprobe. Figure 48 shows the surface topology and Figure 49 shows the microprobe x-ray output scan for As, Te, and Ge. Compare this with Figure 24 that is for the evaporated samples and for water quenched border samples and for air quenched central glassy region samples. To avoid the phase separation in Figure 49, water quenching should be used.

In general, the surfaces of crystalline samples were far rougher than the amorphous samples. Some amorphous samples appeared to be as rough as the crystalline state for another

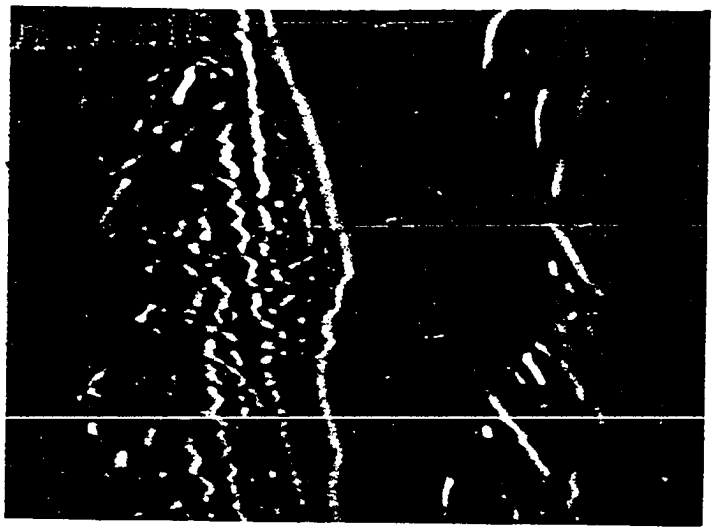

Figure 48. Surface topology of bulk sample E that was air quenched (834X)

Figure 49. Microprobe data for bulk sample E that was air quenched

a. Arsenic scanned x-ray output (834X)

b. Tellurium scanned x-ray output (834X)

c. Germanium scanned x-ray output (834X)

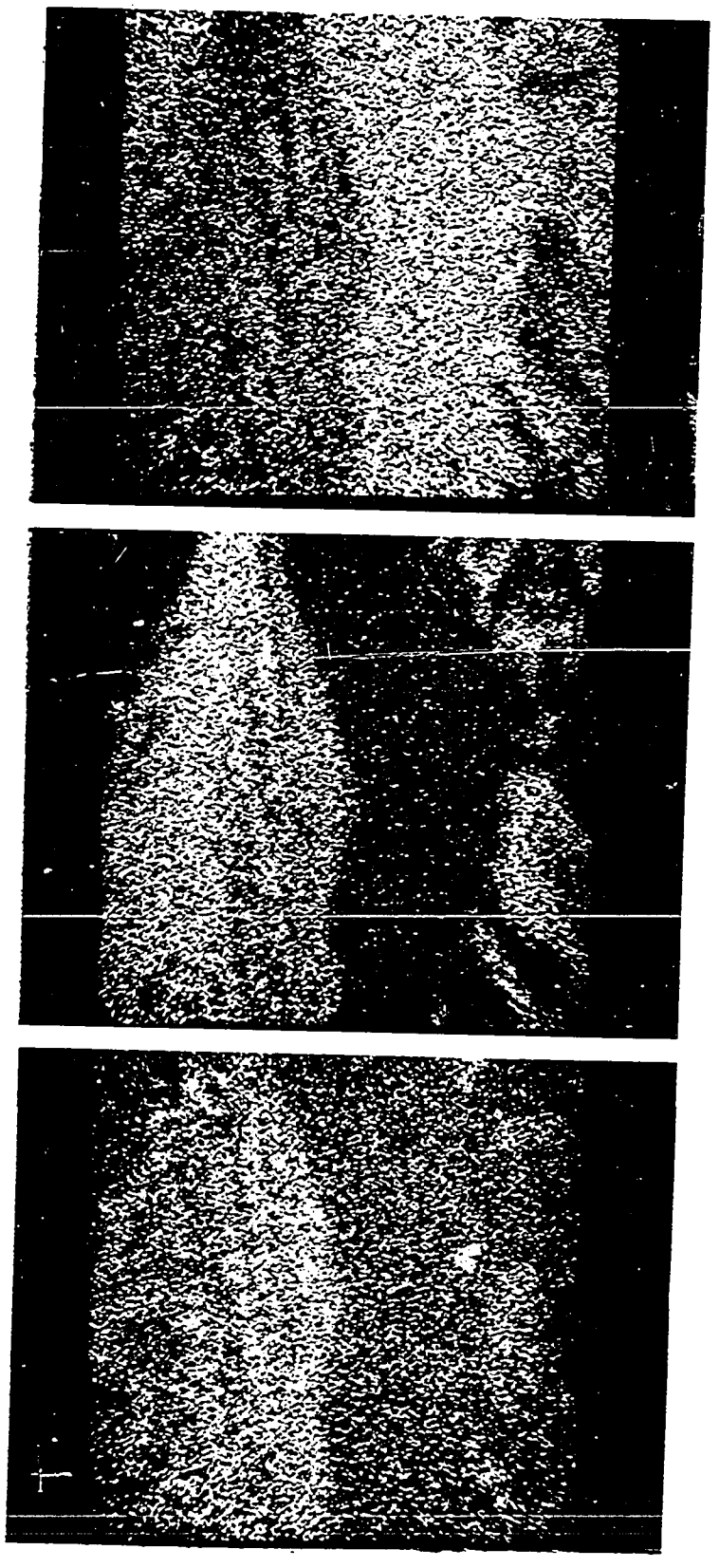

sample. The visual inspection of the samples surface along with the resistivity of the samples provided adequate verification of the state of each sample. X-ray diffraction analysis was not performed because polycrystalline diffraction patterns provide very little useful information.

The tilting of the samples from 0° to 45° added considerable contrast. Figure 25 shows the affect of scanning the surface at a higher magnification. The amorphous state of sample B on a glass substrate looked identical to that of sample A. The crystalline state of sample B was by far the roughest of all the samples. Adhesion to the glass substrate would be affected by this structural effect and explains, perhaps, why the glass substrate samples peeled for this composition.

Sample C's amorphous state exhibited the greatest difference between the glass substrate and the stainless steel substrate. In all other cases the two surfaces were practically identical and, hence, many of these pictures have not been included.

Makedonskii and Pustovoit (17) have found that the secondary yield will be large for materials where $\chi/\Delta E$ is small. χ is the electron affinity and is the energy required to transfer an electron from the bottom of the conduction band to vacuum. ΔE is the band gap energy. They reported $\chi/\Delta E > 2$ for Sb_2S_3 and Sb_2Se_3 and found δ_{max} to be for the

amorphous samples 1.10-1.35 and 1.2-1.4, respectively. However, single crystal NaCl had a δ_{max} of 14.5 and $\chi/\Delta E < 1$. If $\chi/\Delta E$ were known, then perhaps the relatively good yield of the chalcogenide glass samples investigated could be explained.

Böer (2) has worked with a model to explain the conductivity characteristics of disordered semiconductors. In homogenous glasses there are no crystallite boundaries, but the high density of localized defects allows for large potential perturbations, which act similar to those boundaries between microcrystallites. Hence, the amorphous and polycrystalline states can be quite similar. The production of a free electron in the case of glasses is at an energy greater than the potential perturbations, otherwise, the electron is still trapped and does not add to the conductivity. In the polycrystalline case it is at an energy greater than the potential barrier between microcrystallites. The point here is that for this model of disordered semiconductors χ and ΔE are approximately equal and the ratio $\chi/\Delta E \simeq 1$. This implies a high yield because secondaries have a high escape probability. In both cases many secondaries are generated as in a metal but end up being retrapped due to having an energy insufficient to overcome the surface barrier.

The reason why the emission is greater for polycrystalline phases than the amorphous phases can be explained if the structure of each is analyzed in greater detail. In the amorphous

state the potential perturbations due to the high density of localized defects is not a constant but is somehow distributed. Consequently, a secondary in one locality may be trapped in another. According to Böer (2), the mean free path length of a conduction electron in an amorphous material is on the order of 100 angstroms. The polycrystalline structure is ordered over a much larger spatial dimension and this means that the conduction electron's mean free path length is greater. Hence, the escape probability is greater for the polycrystalline phase.

In summary then, the generation of secondaries is greater for the amorphous state because of the large number of loosely bound electrons, the escape to the surface is greater for the polycrystalline state because of its band gap, and the escape from the surface is greater for the amorphous state because of its smoothness.

The increased escape depth may cancel the effects of decreased generation and increased surface roughness producing the results of samples A, D and G. Or the escape depth may dominate as in the remainder of the samples reported. The results of Chen and Wang (4) may be explained by the reverse occurring in that the escape depth change is minimal.

It is interesting to note that the threshold voltage versus film thickness as reported by Stocker, Barlow and Weirauch (28) varies from 25 volts to 40 volts when film

thickness varies from 0.5 microns to 3 microns. The first crossover voltage E_1 also varied for these samples from 20 volts to 40 volts as shown in Table 3.

Future research should be pursued in the area of further evaluation of sample composition's durability, reliability and stability. The peeling problem of some of the samples may not be a problem for memories that are fabricated after the work of Chen and Wang (4).

The research into negative electron affinity (NEA) devices is summarized by Williams and Tietjen (33) and has so far been limited in applications to photomultipliers and photocathodes. The appealing aspect of NEA devices is that $\delta_{max} = 950$ for 20 keV electrons on silicon coated with cesium oxide. Perhaps, NEA devices could be fashioned from chalcogenide glasses and provide a much larger change in the secondary emission characteristics for the two phases.

V. CONCLUSIONS

The application of these glasses to the electron beam memory field is dependent upon the ability to sense the state of the glass. It was the intent of this thesis to determine if amorphous glass materials have a sufficiently large change in δ to allow sensing in this way and to demonstrate an application to computer memories. The results clearly show a large change in the secondary emission characteristics sufficient for computer applications for some of the compositions when they are switched from one phase to another. The polycrystalline state δ_{max} was always equal to or greater than that for the amorphous state for the specified compositions. The crystalline state had a rougher surface than the amorphous state. The high secondary yields implied that the electron affinity and the band gap energy are approximately equal in value. No trends developed as to the means whereby the secondary yields could be predicted as a function of first crossover, second crossover, resistivity, resistivity ratio, or atomic composition. This also applied to the first and second crossovers in that they could not be predicted either.

If the "true" secondary electrons were to be used in order to determine the state of a memory cell, then the data presented would not be applicable. The backscattered component would have too high an energy to be picked up by the normal secondary electron analyzers. Normal analyzers have an energy

cutoff of 10 to 50 volts and they would interfere with the electron beam deflection system. However, if the transmitted current is to be analyzed, then this data is pertinent. In particular, the sensing of a small memory cell must occur at a relatively high voltage or else the electron beam can not be properly focused. A voltage of 4,000 to 5,000 volts must be used for good electron beam characteristics. Samples B, H, I and J are clearly adequate in this voltage range. They have a difference of 1000 to 1600 volts between their second crossovers for the two phases. If, for example, the incident electrons were at 4000 volts, then the sensing of the transmitted current need only be done as to the direction. If the state were amorphous, then $\delta < 1$ and the current direction is negative. If the state were polycrystalline, then $\delta > 1$ and the current direction is positive. The electron beam could be scanned across the memory element and a positive pulse of current would indicate a polycrystalline state and no change would indicate amorphous. These compositions with a large change in E_2 are near the glassy region boundary and are almost in a line at a small germanium content of 4 to 8 atomic percent.

Sample B had the highest order, Figure 30, and the switched samples peeled off of the glass substrates. Sample G being near B in composition also had peeling trouble on the glass, as well as, the stainless steel substrates. The implication here is that G may also be a highly ordered state that leads to large crystallites and poor adhesion.

VI. BIBLIOGRAPHY

1. Barut, A. O. The mechanism of secondary electron emission. Phy. Rev. 93, No. 5: 981-984. 1954.

2. Böer, K. W. The electrical conduction mechanism in highly disordered semiconductors. J. of Non-Cry. Solids 2: 444-453. 1970.

3. Bruining, H. Physics and Applications of Secondary Electron Emission. New York, New York, McGraw-Hill Book Co., Inc. 1954.

4. Chen, A. C. M. and Wang, J. M. An amorphous semiconductor electron beam memory. IEEE Trans. on Mag-8, No. 3: 312-314. Sept. 1972.

5. Chen, A. C. M., Norton, J. F., and Wang, J. M. Secondary electron emission of amorphous semiconducting thin films. App. Phys. Lett. 18, No. 9: 443-444. 1971.

6. Dekker, A. J. Secondary electron emission. Edited by F. Seitz, and D. Turnbull in Solid State Physics. New York, New York, Academic Press. 1958. Vol. 6.

7. Dekker, A. J. Solid State Physics. Englewood Cliffs, N.J., Prentice-Hall, Inc. 1965.

8. Dobretsov, L. N. Secondary electron emission. Acad. of Sci. of the USSR Bull. (Physical Series) 20, No. 9: 899-911. 1956.

9. Geyer, K. H. Beobachtungen an der sekundärelektronenstrahlung aus nichtleitern. Ann. Phys. 42, No. 4: 241-253. 1942.

10. Handel, K. J., Jensen, A. S. and Siedband, M. P. A two electron gun technique for the measurement of secondary emission characteristics of a variety of materials. IEEE Trans. on Elec. Dev., ED-13, No. 6: 525-528. June 1966.

11. Hilton, A. R., Jones, C. E. and Brau, M. Non-oxide IVA-VA-VIA chalcogenide glasses, Part 1. Glass-forming region and variations in physical properties. Phys. and Chem. of Glasses 7, No. 4: 105-112. 1966.

12. Kao, Ven-che. Filament formation in bulk samples of amorphous chalcogenide $As_{55}Te_{35}Ge_{10}$. Unpublished Ph.D. thesis. Ames, Iowa, Library, Iowa State University. 1972.

13. Kaplan, I. Nuclear physics. 2 ed. Reading, Mass., Addison-Wesley Publishing Co., Inc. 1962.

14. Kosmala, A. L., Green, J. P. and Martin, F. H. Engineering Study for a Mass Memory System for Advanced Spacecrafts: Final Report. Intermetics, Inc., Cambridge, Mass. August, 1970.

15. Krebs, H. and Fischer, P. Electrical conductivity of melts and their ability to form glasses in the system Ge+As+Te. Faraday Soc. Discussion 50: 35-44. 1970.

16. Maissel, L. I. and Glang, R. Handbook of Thin Film Technology. New York, McGraw-Hill Book Co., Inc. 1970.

17. Makedonskii, V. I. and Pustovoit, A. K. Secondary electron emission from antimony chalcogenides. Sov. Phys. Solid State 4, No. 8: 1490-1493. 1963.

18. Makedonskiy, V. I. The secondary electron emission of some oxides and chalcogenides of groups III, IV, and V. Radio Engng. Electronics Phys. 10, No. 3: 440-443. 1965.

19. Miller, J. R. Communication Handbook, Part II. Dallas, Texas, Texas Instrument, Inc., Semiconductor Component Div. 1965.

20. Ooka, K., Dunn, B. and Mackenzie, J. D. Secondary electron emission from glass and its practical applications. J. of Non-Cry. Solids 12: 1-17. 1973.

21. Richards, R. K. Digital Computer Components and Circuits. Princeton, New Jersey, D. Van Nostrand Co., Inc. 1957.

22. Robertson, J. M. and Owen, A. E. Physical factors affecting switching in chalcogenide films. Symposium on Electrotechnical Glasses. Soc. of Glass Tech., Imperial College, London, England. 1970.

23. Rudberg, E. Inelastic scattering of electrons from solids. Phys. Rev. 50: 138-150. 1936.

24. Salow, H. Über den sekundäremissionsfaktor elektronenbestrahlter isolatoren. Z. Tech. Phys. 21, No. 1: 8-15. 1940.

25. Shul'man, A. R. Secondary-electron emission of dielectrics and metals. Acad. of Sci. of the USSR Bull. (Physical Series) 20, No. 9: 912-924. 1956.

26. Sie, C. H. Memory cell using bistable resistivity in amorphous As-Te-Ge film. Unpublished Ph.D. thesis. Ames, Iowa, Library, Iowa State University of Science and Technology. 1969.

27. Simpson, J. A. Design of retarding field energy analyzers. The Rev. of Scientific Inst. 32, No. 12: 1283-1288. 1961.

28. Stocker, H. J., Barlow, C. A., Jr. and Weirauch, D. F. Mechanism of threshold switching in semiconducting glasses. J. of Non-Cry. Solids 4: 523-525. 1970.

29. Uttecht, R. R., Stevenson, H., Sie, C. H., Griener, J. D. and Raghavan, K. S. Electric field-induced filament formation in As-Te-Ge glass. J. of Non-Cry. Solids 2: 358-370. 1970.

30. Warren, A. C. Switching mechanism in chalcogenide glasses. Elec. Lett. 5, No. 19: 461-462. 1969.

31. Warren, A. C. and Male, J. C. Field-enhanced conductivity effects in thin chalcogenide switches. Elec. Lett. 6, No. 18: 567-569. 1970.

32. Whetten, N. R. Secondary electron emission. Eds, Hughes, V. W. and Schultz, H. L. Atomic Sources and Detectors, Vol. 4, Part A: 69-84. New York, New York, Academic Press, Inc. 1967.

33. Williams, B. F. and Tietjen, J. J. Current status of negative electron affinity devices. Proc. of the IEEE 59, No. 10: 1489-1497. October 1971.

VII. ACKNOWLEDGMENTS

I want to thank Professor Art V. Pohm of the Electrical Engineering Department, Iowa State University, for suggesting this topic and for his guidance and counseling in the pursuit of it. I also wish to thank Professor Chester Comstock of the Electrical Engineering Department, Iowa State University, for his help in the experimental work, and Terry McConnell and the machine shop "crew" of the Electrical Engineering Department's machine shop, Iowa State University, for their help in building many experimental setups.

This work would not have been performed without the financial benevolence of the Solid State Affiliate Program of the Engineering Research Institute, Iowa State University.

Last but most importantly, I want to thank my wife whose patience and understanding helped to make this work a reality.